Combined Impacts of Nitrous Acid and Nitryl Chloride on Lower Tropospheric Ozone: New Module Development in WRF-Chem and Application to China

Li Zhang [1], Qinyi Li [1], Tao Wang [1,*], Ravan Ahmadov [2,3], Qiang Zhang [4], Meng Li [4], and Mengyao Lv [5]

[1] Department of Civil and Environmental Engineering, The Hong Kong Polytechnic University, Hong Kong, China,

[2] Cooperative Institute for Research in Environmental Sciences, University of Colorado at Boulder, Boulder, CO, USA,

[3] Earth System Research Laboratory, National Oceanic and Atmospheric Administration, Boulder, CO, USA,

[4] Department of Earth System Science, Tsinghua University, Beijing, China,

[5] National Meteorological Center, China Meteorological Administration, Beijing, China

[*] *Correspondence to:* T. Wang (cetwang@polyu.edu.hk)

Abstract. Nitrous acid (HONO) and nitryl chloride ($ClNO_2$)—through their photolysis—can have profound effects on the nitrogen cycle and oxidation capacity of the lower troposphere. Previous numerical studies have separately considered and investigated the sources/processes of these compounds and their roles in the fate of reactive nitrogen and the production of ozone (O_3), but their combined impact on the chemistry of the lower part of the troposphere has not been addressed yet. In this study, we updated the WRF-Chem model with the currently known sources and chemistry of HONO and chlorine in a new chemical mechanism (CBMZ_ReNOM), and applied it to a study of the combined effects of HONO and $ClNO_2$ on summertime O_3 in the boundary layer over China. We simulated the spatial distributions of HONO, $ClNO_2$, and related compounds at the surface and within the lower troposphere. The results showed that the modeled HONO levels reached up to 800–1800 ppt at the surface (0–30 m) over the Northern China Plain (NCP), the Yangtze River Delta (YRD), and the Pearl River Delta (PRD) regions and that HONO was concentrated within a 0–200 m layer. In comparison, the simulated surface $ClNO_2$ mixing ratio was around 800–1500 ppt over the NCP, YRD, and central China regions and was predominantly present in a 0–600 m layer. HONO enhanced daytime RO_x ($OH+HO_2+RO_2$) and O_3 at the surface (0–30 m) by 2.8–4.6 ppt (28–37%) and 2.9–6.2 ppb (6–13%), respectively, over the three most developed regions, whereas $ClNO_2$ increased surface O_3 in the NCP and YRD regions by 2.4–3.3 ppb (or 5–6%) and it also had a significant impact (3–6%) on above-surface O_3 within 200–500 m. The combined effects increased surface O_3 by 11.5%, 13.5%, and 13.3% in the NCP, YRD and PRD regions, respectively. Over the boundary layer (0–1000m), the HONO and $ClNO_2$ enhanced O_3 by up to 5.1% and 3.2%, respectively, and their combined effect increased O_3 by 7.1–8.9% in the three regions. The new module noticeably improved

O$_3$ predictions at ~900 monitoring stations throughout China by reducing the mean bias from -4.3 ppb to 0.1 ppb. Our study suggests the importance of considering these reactive nitrogen species simultaneously into chemical transport models to better simulate the formation of summertime O$_3$ in polluted regions.

1 Introduction

5 Reactive nitrogen compounds play important roles in atmospheric chemistry and affect the formation of secondary pollutants including ozone (O$_3$) and secondary aerosols. In recent decades, nitrous acid (HONO), dinitrogen pentoxide (N$_2$O$_5$), and nitryl chloride (ClNO$_2$) have received considerable attention, together with the traditionally known oxides of nitrogen (NO+NO$_2$), due to their potentially significant impact on the oxidation capacity in the polluted portion of the troposphere (Brown, 2006; Su et al., 2011; Thornton et al., 2010). HONO can be heterogeneously formed via conversions of NO$_2$ (R1) on

10 particle, land, and sea surfaces (Kleffmann, 2007; Zha et al., 2014), directly emitted by traffic and biological activities (Kurtenbach et al., 2001; Oswald et al., 2013), and formed via photolysis of nitric acid (Zhou et al., 2011). During the day, HONO is then photochemically converted into OH radicals and NO (R2), both of which have an impact on the oxidation capacity (Kleffmann, 2007). N$_2$O$_5$, a night reservoir of NO$_x$, can react on particles containing chloride to form ClNO$_2$ (R3). Within a few hours after sunrise, the ClNO$_2$ is photolyzed into NO$_2$ and reactive chlorine atoms (R4), the latter of which

15 further react with hydrocarbons to produce additional peroxy radicals (RO$_2$ and HO$_2$) and subsequently accelerate the cycling of oxidants in the atmosphere at both ground level and upper levels (e.g. Tham et al., 2016; Wang et al., 2016). The photolysis of HONO and ClNO$_2$ during the daytime could have a significant effect on the formation of secondary pollutants in polluted regions (Osthoff et al., 2008; Tham et al., 2016; Tang et al., 2015; Thornton et al., 2010; Wang et al., 2016).

$$2NO_{2(g)} + H_2O \rightarrow HONO_{(g)} + HNO_{3(g)} \tag{R1}$$

20 $$HONO_{(g)} + h\nu \rightarrow OH^* + NO_{(g)} \tag{R2}$$

$$N_2O_{5(g)} + Cl^-_{(aq)} \rightarrow ClNO_{2(g)} + NO_3^-_{(aq)} \tag{R3}$$

$$ClNO_{2(g)} + h\nu \rightarrow Cl^*_{(g)} + NO_{2(g)} \tag{R4}$$

Previous numerical studies have separately considered the sources/processes of HONO and ClNO$_2$-initiated chlorine chemistry and investigated their respective effects on O$_3$ in different regions. By considering direct and secondary HONO

25 sources, a few studies using regional chemical transport models (e.g. CMAQ, WRF-Chem) suggested that HONO could enhance surface-level O$_3$ by 1.4–6 ppb in North America (Li et al., 2010; Sarwar et al., 2008), 1–3 ppb in Europe (Elshorbany et al., 2012; Gonçalves et al., 2012), and 3–12 ppb in northern China (Li et al., 2011; An et al., 2013). A very recent study by our group parameterized up-to-date HONO sources, including gas-phase reactions, heterogeneous formation

at various surfaces, traffic sources, and biological emissions, into a chemistry transport model (WRF-Chem). The improved model well reproduced the HONO observed at a suburban site with complex terrain in Hong Kong and indicated an enhancement of 10–12% in ground-level O_3 concentration over the Pearl River Delta region (PRD), China (Zhang et al., 2016).

5   Several chemical transport model studies have evaluated the impact of the hydrolysis of N_2O_5, the subsequent formation of $ClNO_2$, and/or Cl-radical-initiated chemistry on tropospheric chemistry in North America and Europe. These studies suggested that the new chemistry could influence NOx and chlorine cycling, leading to an enhancement of 1−2 ppb in surface O_3 concentration in Texas (Simon et al., 2010), a 3–4% increase in monthly average 8-h O_3 across the U.S. (Sarwar et al., 2012), and a negative impact on nighttime oxidative chemistry with reductions of up to 30% in NO_3 and N_2O_5 (without

10   considering chlorine chemistry) over the north-western Europe (Archer-Nicholls et al., 2014; Lowe et al., 2015). In a recent study, we parameterized the heterogeneous uptake of N_2O_5, the formations of $ClNO_2$, and chlorine chemistry into WRF-Chem, and demonstrated that these processes could lead to O_3 enhancement of up to 16.3% within the planetary boundary layer (PBL) over the PRD region in the winter season (Li et al., 2016).

Despite the above-mentioned research on the effects of HONO and $N_2O_5/ClNO_2$, a comprehensive assessment of their

15   combined impacts on O_3 is lacking. The sources (and thus the impacts) of HONO are mostly near the ground surface (Su et al., 2011; Zhang et al., 2016), whereas significant amounts of $ClNO_2$ form within the residual layer and can be transported to the surface level in the morning after breakup of the nocturnal inversion layer (Tham et al., 2016; Wang et al., 2016). Moreover, the chemical processes of HONO and $N_2O_5/ClNO_2$ occur concurrently and interact with each other in the troposphere, both of which would simultaneously shift the composition of the total reactive nitrogen (NO_y), influence the

20   nitrogen oxide chemistry, and affect the formations of secondary pollutants. To the best of our knowledge, no global or regional models, however, have simultaneously considered the sources/processes of HONO and $ClNO_2$ and evaluated their regional combined impacts on the formation of O_3 pollution in the boundary layer of the atmosphere.

In the present study, we developed a new chemical mechanism option in WRF-Chem to consider both the detailed HONO sources/processes and chlorine chemistry and applied the new mechanism to investigate their respective and combined

25   effects on summertime O_3 pollution in the lower troposphere over China. In the remainder of this paper we describe the new developments in WRF-Chem, detailed model configurations, and measurement data used in the study in section 2. Then, in section 3, we show the model simulations of HONO, N_2O_5, and $ClNO_2$ over China during a 12-day period in summer and compare the results against available measurements. Following this, we illustrate the impacts of HONO and $ClNO_2$ on O_3 pollution in China. The major findings of the study are given in section 4.

2 Methodology

2.1 Development of CBMZ_ReNOM

A new chemical mechanism option in WRF-Chem, namely CBMZ_ReNOM, was further developed based on the CBMZ mechanism to include detailed HONO chemistry and chlorine chemistry in this study. The CBMZ gas-phase chemical mechanism was developed by Zaveri and Peters (1999). It treats 67 species and 164 reactions using a lumped-structure approach that categorizes organic compounds according to the types of bonds present in their molecular structures. The original mechanism does not contain any direct emissions or secondary formation of HONO except for the well-known homogeneous formation via OH and NO, nor does it consider any chemical reactions involving chlorine-containing species. We incorporated the following new chemistry into the CBMZ_ReNOM module based on the CBMZ mechanism.

2.1.1 HONO chemistry

In our previous study, we expanded the original CBMZ mechanism by adding up-to-date comprehensive sources of HONO, including gas-phase formations (in addition to the reaction between OH and NO), heterogeneous formations, direct traffic sources, and soil bacteria emissions as described by Zhang et al. (2016). We showed that including these additional sources of HONO very well simulated the observed HONO at a suburban site in southern China. In this study, we added similar HONO-related processes, which are briefly summarized below.

Heterogeneous formations

$$NO + NO_2 + H_2O \xrightarrow{surface} 2HONO \qquad (k_5 = 4.4 \times 10^{-40}) \tag{R5}$$

$$2HONO \xrightarrow{surface} NO + NO_2 + H_2O \qquad (k_6 = 1.0 \times 10^{-20}) \tag{R6}$$

$$NO + HNO_3 \xrightarrow{surface} HONO + NO_2 \qquad (k_7 = \tfrac{1}{4} \cdot v_{NO} \cdot \left(\tfrac{S}{V}\right) \cdot \gamma_{NO}) \tag{R7}$$

$$2NO_2 + H_2O \xrightarrow{surface} HONO + HNO_3 \qquad (k_8 = \tfrac{1}{4} \cdot v_{NO_2} \cdot \left(\tfrac{S}{V}\right) \cdot \gamma_{NO_2}) \tag{R8}$$
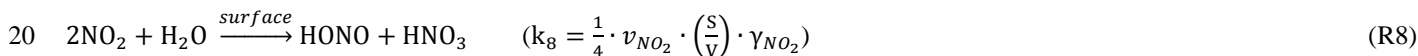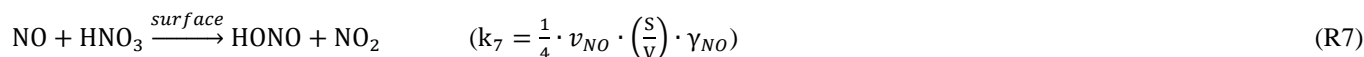
All of the heterogeneous reactions were considered as simple first-order reactions and the formed HONO was assumed to out-gas instantaneously. The reaction rates for the reaction between nitric oxide and nitrogen dioxide on wet surface (R5) and the surface-mediated self-reaction of HONO (R6) were obtained from Kaiser and Wu (1977b, 1977a). The first-order reaction rates for R7-8 were estimated following the recommendations in Zhang et al. (2016), where v is the mean molecular velocity of given reactant (m s^{-1}), S/V is the surface to volume ratio (m^{-1}) calculated by using the method in Zhang et al.

(2016), and γ is the uptake coefficient of reactant with a constant value of 1×10^{-8} being used for R7 (Rivera-Figueroa et al., 2003) and light density dependent values as introduced in Zhang et al. (2016) being employed for R8.

Direct emissions

The model also considers HONO directly emitted from anthropogenic sources (vehicles and water vessels) and biological activities. A widely-used traffic emission ratio of 0.8% (ratio of HONO to NO_x in the traffic emission sector) was applied to parameterize traffic emission of HONO (Kurtenbach et al., 2001; Sarwar et al., 2008). For direct emissions from soil bacteria, we followed the parameterization of Zhang et al. (2016) with consideration of the dependence on land category, soil humidity, and temperature. In brief, we first mapped the optimum HONO emission fluxes of various soil categories (from 17 ecosystems) measured by Oswald et al. (2013) into the most closely matching United States Geological Survey (USGS) land categories in the WRF-Chem model following the mapping schemes described by Zhang et al. (2016). Then, the emission flux for each USGS land-use type was calculated as the aggregation of the measured fluxes from the measured category/categories that was/were mapped into the specific USGS classifications. After that, the optimum fluxes over the domain were incorporated into the model and were further scaled online according to the soil temperature and water content in each model grid at each time step throughout the simulation period. More details of the parameterization can be found in Zhang et al. (2016).

2.1.2 Heterogeneous N_2O_5 chemistry and chlorine chemistry

For the heterogeneous formation of $ClNO_2$ through the reactions of N_2O_5 on Cl-containing particles, we applied the modified MOSAIC module developed by Archer-Nicholls et al. (2014) and Lowe et al. (2015). The heterogeneous processes of N_2O_5 were considered as simple first-order reactions, taking into account the particle surface area density, molecular velocity, and uptake coefficient of N_2O_5 on an aerosol surface. Parametrization of the uptake coefficient of N_2O_5 and the yield of $ClNO_2$ followed the methods reported by Roberts et al. (2009) and Bertram and Thornton (2009) and further considered its suppression by organic coatings using the method proposed by Riemer et al. (2009). More details on the modifications were introduced by Archer-Nicholls et al. (2014) and Lowe et al. (2015).

In the treatment of heterogeneous N_2O_5 chemistry in WRF-Chem by Archer-Nicholls et al. (2014), $ClNO_2$ was assumed to out-gas near-instantaneously, and it was treated as an inert species without further gas-phase reactions. Based on their development, we further included the chlorine chemical reactions listed in Table 1 into the CBMZ_ReNOM module. The chlorine mechanism introduced in the present study further extends the one proposed by Sarwar et al. (2012), which was based on CB05, and includes more chlorine species and reactions. It consists of six photolysis reactions (photolysis of Cl_2, HOCl, $ClNO_2$, $ClONO_2$, and FMCl) and 30 gas-phase reactions (R7–R36 as listed in Table 1), and introduces seven new chemical species (Cl, Cl_2, ClO, HOCl, $ClNO_2$, $ClONO_2$, and FMCl) into the original CBMZ mechanism. The reactions

between lumped volatile organic compounds (VOCs) species and Cl radicals are similar to their reactions with OH radicals (Table 1).

2.1.3 Photolysis module

The photolysis rates of the newly added chlorine-containing chemicals, i.e., Cl_2, HOCl, $ClNO_2$, $ClONO_2$, and FMCl (reactions 1–6 in Table 1), in the CBMZ_ReNOM module were considered in both the Fast-J and Madronich photolysis modules in WRF-Chem. The photolysis rates were calculated using Eq. (1), which depends on the quantum yield (ϕ) and absorption cross-section (σ) of each chemical species (*i*), as functions of wavelength and temperature, and on the actinic flux (F), as a function of solar radiation and wavelength.

$$J_i = \int \phi_i(\lambda, T)\sigma_i(\lambda, T)F(\lambda)d\lambda \quad (1)$$

The absorption cross sections and quantum yields for the reactions were obtained from the atmospheric chemical kinetic database of the International Union of Pure and Applied Chemistry (http://iupac.pole-ether.fr/) and were interpolated into the wavelengths that used in the Fast-J and Madronich modules, while the actinic flux was calculated in the photolysis modules (Wild et al., 2000; Madronich, 1987). Only the modified Fast-J module was applied for providing the photolysis rates in the present study.

2.2   WRF-Chem model set up

2.2.1 Model configurations

The three-dimensional Weather Research and Forecasting coupled with Chemistry (WRF-Chem) model (https://ruc.noaa.gov/wrf/wrf-chem/) simulates the transport, mixing, and chemical transformation of trace gases and aerosols simultaneously with meteorology (Grell et al., 2005). The chemical mechanism used to simulate the gases and aerosols is based on the CBMZ/CBMZ_ReNOM module coupled with the sectional Model for Simulating Aerosol Interactions and Chemistry (MOSAIC, Zaveri et al., 2008) with new parameterizations of the heterogeneous uptake of N_2O_5 and $ClNO_2$ formation (Archer-Nicholls et al., 2014). Other major physical and chemical schemes applied in our WRF-Chem simulations included the Goddard shortwave radiation scheme (Chou et al., 1998), the rapid radiative transfer model (RRTM) long-wave radiation scheme (Mlawer et al., 1997a), the Mellor-Yamada-Janjic (MYJ) PBL scheme (Janjić, 1994), the modified double-moment version of the Lin microphysics scheme (Lin et al., 1983), and the Grell-Dévényi cumulus scheme (Grell and Dévényi, 2002) (see Table 2). The simulation domain in this study was designed to cover most of China with a resolution of 27×27 km as illustrated in Figure 1. The vertical resolution included 31 layers with a fixed-model top pressure of 100 hPa, with the first model layer set to be about 30 m above ground level (a.g.l.) and eight model layers below 1000 m a.g.l. (approximately the height of PBL at noon). Simulations by the Model for Ozone and Related Chemical Tracers (MOZART,

version 4) driven by Goddard Earth Observing System-5 fields were used to provide the initial and boundary conditions for WRF-Chem (Emmons et al., 2010). Note that the MOZART-4 model does not treat chlorine chemistry nor considers any HONO sources.

Four simulation cases were designed, as listed in Table 3. In the base case, the default WRF-Chem model was employed. The ReNOM_HONO and ReNOM_Cl cases applied the new CBMZ_ReNOM module considering HONO chemistry and Cl-chemistry individually, respectively, whereas in the ReNOM case, the CBMZ_ReNOM module with both HONO and Cl-initiated reactions was used. A period during the summer season (26 June-7 July 2014) was selected for model simulations because ozone pollution is severe in the summer in most regions of China (Wang et al., 2017). The first 24 h of the simulation were considered as a spin-up time. The four-dimensional nudging-based data assimilation method was used in our WRF-Chem simulations throughout the simulation period. This method effectively improves the meteorological performance of WRF-Chem (Zhang et al., 2015; Zhang et al., 2016). Meteorological observations at more than 3614 surface stations (tri-hourly) and 297 sounding stations (12-hourly) were obtained from the China Meteorological Administration and integrated into the simulations through observational nudging (Figure 1a). National Centers for Environmental Prediction final reanalysis data (https://rda.ucar.edu/datasets/ds083.2/) were used in the analytical nudging.

2.2.2 Emission data

Three sets of anthropogenic emission inventories were used in our simulations. For mainland China, we applied the latest Multi-resolution Emission Inventory for China (MEIC) in 2013 with a resolution of $0.25° \times 0.25°$. The MEIC provides the monthly emissions of ten primary anthropogenic pollutants, including sulphur dioxide (SO_2), nitrogen oxides (NOx), carbon monoxide (CO), ammonia (NH_3), particulate matter with diameter less than/equal to 2.5 μm ($PM_{2.5}$), particulate matter with diameter less than/equal to 10 μm (PM_{10}), black carbon (BC), organic carbon (OC), and nonmethane volatile organic compounds (NMVOCs), from the five major sectors of agriculture, industry, power plants, residential, and transportation (http://www.meicmodel.org). The emission inventory was developed by Tsinghua University based on a technology-based emission model (Lei et al., 2011; Zhang et al., 2009), and this inventory has been suggested to offer reasonable model predictions of $PM_{2.5}$ and O_3 in multiple cities over China during multiple years (Zhang et al., 2015; Zhang et al., 2016). For other Asian regions, the emission inventory for Asia (MIX) in 2010 with a resolution of $0.25° \times 0.25°$ was used in the simulations. The MIX emission inventory was developed for the Model Inter-Comparison Study for Asia (MICS-Asia) and covers all major anthropogenic sources in 30 Asian countries and regions (Li et al., 2017). More details of the MIX emission inventory can be found in (Li et al., 2017), and monthly emission datasets are available at http://www.meicmodel.org/dataset-mix. For chlorine emissions, the Reactive Chlorine Emission Inventory (RCEI; Keene et al. (1999) and references therein) was adopted. The RCEI, on a of $1° \times 1°$ grid scale, contains emissions of a total of nine reactive chlorine species from both biomass burning and anthropogenic activities. Although the RCEI might be subject to large uncertainties in terms of representing Cl emissions in China due to its low spatial resolution and obsolete surrogate data (in 1990), as discussed in Li

et al. (2016), we still applied this emission inventory because it is the only Cl emission inventory currently available for China. Diurnal, day-of-week, and vertical allocations of the emissions followed the methods introduced by Zhang et al. (2015). For natural emissions, the Model of Emissions of Gases and Aerosols from Nature version 2.1 (MEGAN) (Guenther et al., 2006) was used to calculate the biogenic emissions over the domain throughout the simulation period.

2.2.3 O_3 and NO_2 measurement data

Real-time measurements of ground-level O_3 and NO_2 were conducted routinely at ~1000 stations in the national air quality monitoring network that was established by the Ministry of Environmental Protection (MEP) of China since 2013. The MEP has operated this monitoring network and made the data publically available at http://106.37.208.233:20035/ since 2013. The measurements were conducted at local environmental protection bureaus in each city following the same standards for instrument operation and quality control set by the China MEP (http://www.mep.gov.cn/). Hourly data from 908 surface stations were available during our simulation period and used in this study (Figure 1b). It should be noted that NO_2 measurements in MEP's network, as in regulatory networks of other countries, were made with the catalytic conversion of NO_2 to NO. This method is known to overestimate NO_2, especially during the photochemically active daytime and in locations away from the sources of emissions (Xu et al., 2013).

3   Results and Discussion

3.1   Simulated HONO, N_2O_5, and $ClNO_2$ with the CBMZ_ReNOM over China

3.1.1 Spatial and vertical distributions of HONO

In Figures 2a and 2b, we show the spatial distributions of the surface NO_2 and HONO concentrations, respectively, simulated by the CBMZ_ReNOM module. During the simulation period, NO_2, the main precursor of HONO and N_2O_5, was, overall, reasonably reproduced by our model compared with the observations as shown in Table S1 and Figure S1. The over-simulations of NO_2 over the YRD was due to the possible overestimates in NO_x emissions: e.g. annual NO_x emission estimated by the MEIC in 2010 over the YRD region (including Jiangsu, Shanghai, and Zhejiang provinces) was much larger than the estimate by Fu et al. (2013) with a much higher resolution (4×4 km) over the same region (3749 vs. 2777 kt in annual average). It can be observed in Figure 2 that high levels of HONO were simulated over the NCP and YRD regions, with values of 800–1400 ppt and 1000–2000 ppt, respectively. Over central China (mostly Jiangxi and Hubei provinces) and the PRD, HONO reached up to 1000 ppt during the simulated period. Similar spatial distributions of simulated HONO were also reported by Tang et al. (2015), who considered several heterogeneous sources, traffic emissions, and an unknown source of HONO, and simulated 0.5–2.5 ppb of HONO over the NCP, YRD, and PRD regions during two summer seasons (Jul 2006 and Aug 2007). An interesting phenomenon is that high concentrations of HONO are simulated in Taiwan, Korea, and

southern Japan. There may be two reasons for these results. Firstly, these regions had high NO_x emissions and high NO_2 concentrations (up to 30 ppb during the simulation period, as illustrated in Figure 2a and Figure S1). Second, these regions are covered with large areas of vegetation that are mapped with high soil bacterial emissions (agriculture lands, shrubs, and woody lands), as measured by Oswald et al. (2013). Comparisons between the model simulations of HONO and the limited observations in these regions will be discussed in section 3.2.

Figures 3a and 3b illustrate the vertical distributions of NO_2 and HONO across the NCP region and central China, respectively, during nighttime. The model predicted elevated HONO concentrations with values of 350–700 ppt over the NCP region and central China where high NO_2 concentrations are present. It can be seen in Figures 3b and 4b that the modeled HONO was mostly concentrated near the surface (0–200 m) within the PBL over the three most concerned regions (NCP, YRD, and PRD) in China. This is due to two reasons. One is that NO_2, the main precursor of HONO, is highly concentrated within this layer (Figure 4a) and the heterogeneous formation at ground surface is the dominant source of HONO in the atmosphere as suggested in previous studies (Zhang et al., 2016; Li et al., 2010). The other reason is that the direct HONO emissions, including the soil bacterial emission and traffic emission, were also within the near-surface layer.

3.1.2 Spatial and vertical distributions of N_2O_5 and $ClNO_2$

Figures 2c and 2d show the simulated spatial distributions of N_2O_5 and $ClNO_2$ over East Asia. It can be seen that N_2O_5 was highly concentrated in the NCP and YRD regions, with levels of 20–60 ppt at the surface level and 30–100 ppt within the PBL (Figure 3c) over the polluted NCP region and central China during nighttime. Higher N_2O_5 levels were found in the residual layer (of 100–500 m a.g.l.) over the NCP and YRD regions (see Figure 4c). Low N_2O_5 concentrations were simulated over southern China, which is consistent with generally good air quality due to influence of monsoon weather in the summer season (Wang et al., 2009). High levels of $ClNO_2$ in a range of 500–900 ppt were simulated in the NCP and YRD regions, where large amounts of chloride (Figure S2) and NO_x (Figure S1a) are present. The simulated concentrations of $ClNO_2$ in the NCP were generally similar to the results reported by Sarwar et al. (2014), who used a hemispherical chemical transport model with a spatial resolution of 108 km; however, our study gave more refined results at 27 km. Strong heterogeneous production of $ClNO_2$ was also simulated over central China (CC) and Sichuan Basin (SB) with intensive anthropogenic emissions of NO_x and chloride. Up to 800 ppt and 600 ppt of $ClNO_2$ were simulated over the polluted regions (e.g. NCP, YRD, and CC) at the surface and spreading over the boundary layer (Figures 3d and 4d, respectively). The simulated $ClNO_2$ in the Hong Kong-PRD region was lower than those in the NCP, YRD, CC, and SB regions.

3.2 Model performance of HONO and $N_2O_5/ClNO_2$

We compared the simulations of HONO by the new module with field observations reported in Korea, Japan, Taiwan, Hong Kong, and mainland China (see Table 4). As listed, the measured HONO ranged from 0.59 to 2.8 ppb at multiple sites over

China. Over the NCP, YRD, and PRD regions, the model simulations were generally in line with the observed HONO levels, especially those in summer seasons (Table 4). The model very well captured the measured HONO at Wangdu (Tan et al., 2017) in the NCP region with an averaged simulation of 0.81 ppb comparing with a mean observed value of 0.94 ppb during the simulation period. A detailed comparison of the observed and simulated pollutants at Wangdu during the campaign is shown in Table S2 and Figure S3 in the supplementary materials (for details of the campaign, please refer to Tham et al. (2016); Tan et al. (2017) and references therein). The simulations also agreed well with the observations in coastal cities in northern Japan (Sapporo), southeast Japan (Tokushima), and Tokyo. Besides, our modelled HONO were consistent with limited measurements in hot spots in Taiwan, Japan, and Korea (Figure 2b). For instance, Tsai et al. (2014) measured HONO in multiple seasons during 2005-2007 using MOUDI in southern Taiwan (Kaohsiung) and found a HONO concentration of ~2.8 ppb at night and ~1.5 ppb during the day. Simulations of our model (3.3 ppb during nighttime and 1.9 ppb during daytime) were very close to the observations at this site. Kim et al. (2015) observed HONO concentrations up to 1 ppb in a forested area in Seoul, Korea, during the summer and Song et al. (2009) reported HONO concentrations with a maximum value of 8.61 ppb on the campus of the University of Seoul, Korea, between May and July, 2005. The model oversimulated the average HONO in Korea by 3–7 times, but it was able to capture the maximum observed values. The overestimates were probably due to uncertainties in the treatment of soil bacterial emissions over this region. Compared with the model performance reported in previous numerical studies, which reproduced 20–80% of the observed HONO (An et al., 2013; Li et al., 2010; Gonçalves et al., 2012; Elshorbany et al., 2012), the overall performance of HONO of the new module in our model was satisfactory.

Very limited observations of N_2O_5 and $ClNO_2$ have been made in Asia. In Table 4, we summarize the available measurements of N_2O_5 and $ClNO_2$ in Asia, along with the simulated values by our model. As shown, N_2O_5 with a mean value of 7–28 ppt was observed in Mt. Tai, an urban area (Shandong University campus in Jinan) and a semi-rural area (Wangdu) over the NCP region. In Japan, N_2O_5 measurements in Toyokawa were reported by Nakayama et al. (2008), with values of ~20 ppt. The observed $ClNO_2$ values were in the range of 30–160 ppt in Wangdu, Mt. Tai, and Jinan in the northern China. Overall, the simulated values by our new module were of the same order of magnitude as the observed values at the sites in northern China and Japan. During the simulation period, the CBMZ_ReNOM module very well reproduced the average levels of N_2O_5 (observation of 27.9 vs. simulation of 23.9 ppt) and $ClNO_2$ (159.5 ppt vs. 265.6 ppt) observed at the Wangdu site (Tham et al., 2016) in northern China. The detailed comparison between the modelled and observed N_2O_5 and $ClNO_2$ can be found in Table S2 and Figure S3 in the supplementary materials. The observations of N_2O_5 (278 ppt) and $ClNO_2$ (74.6 ppt) at a mountain top site in Hong Kong during winter time were much higher than our model results during the simulation period (Table 4), probably due to (1) the complex terrain of this mountain top site (close to urban area, oceans, and with high altitude, see Brown et al. (2016) and Wang et al. (2016)) which cannot be well resolved by the model at a resolution of 27×27 km; and (2) the differences between the meteorological conditions in the measurement season (winter, with prevailing northerly winds) and those during the simulation period (summer, with mostly southerly winds). But our previous work with

WRF–Chem improved by similar N_2O_5 and $ClNO_2$ parameterizations captured the observations at this site in winter (Li et al., 2016). Compared with the performance of previous model simulations, our results for N_2O_5 and $ClNO_2$ with the newly developed CBMZ_ReNOM module in China were satisfactory. For example, Lowe et al. (2015) oversimulated N_2O_5 by 15–32% due to the uncertainties in meteorological simulations and the treatment of the heterogeneous uptake of N_2O_5. Sarwar et al. (2014) reproduced the observed peak values of $ClNO_2$ by 12–2100% at multiple sites in the northern hemisphere, which was probably because of the relatively low model resolution (108 km). Li et al. (2016) simulated lower N_2O_5 levels within a factor of 3 and higher $ClNO_2$ within a factor of 4 compared to the observations at night in Hong Kong, which were partially due to the underestimated production of N_2O_5, the overestimated uptake of N_2O_5, and incomplete considerations of some possible sinks of $ClNO_2$ (e.g. Roberts et al., 2008) in the model. In the present study, the emissions of NO_x provided by the MEIC may be subject to uncertainties in terms of intensity and spatial distribution (e.g. the possible overestimates over the YRD as we discussed); the chlorine emission in the RCEI that we applied is expected to have large uncertainties due to its low spatial resolution and out-dated emission related data (for 1990) (Keene et al., 1999). For these reasons, our model results of HONO and $ClNO_2$ (and their impacts) inevitably carry uncertainties. More studies are required to refine and update the NO_x and chlorine emissions in China.

3.3 Integrated effects on O_3 in the CBMZ_ReNOM

3.3.1 Enhancements in regional RO_x ($OH+HO_2+RO_2$) and O_3 levels over polluted regions

Figures 5 and 6 show the spatial patterns at the surface (0-30 m) and the vertical distributions of daytime RO_x and O_3 enhancement, respectively, over the three most concerned regions (NCP, PRD, and YRD), respectively. It is noticeable that the added $ClNO_2$ and HONO processes enhanced daytime RO_x across the whole domain. Over the NCP and YRD regions, where the simulated $ClNO_2$ was elevated (Figure 5c), the enhancement in RO_x due to the added chlorine chemistry was up to 1.8 ppt (12.5%) within the PBL (0–1000 m), and it increased with increasing altitude within the 0–500 m layer (see Figures 6a–6f). The releases of reactive Cl atoms and NO_x through the daytime photolysis of $ClNO_2$, which serves as a reservoir of NO_x during nighttime, led to more O_3 production, especially over the NCP and YRD regions. As shown in Figures 6g–6i, $ClNO_2$ increased the surface O_3 in the NCP and YRD regions by 2.4–3.3 ppb (or 5–6%). It also had a significant impact (3-6%) on the 200–1000 layer within the PBL, as also seen in Figure S4. However, over the PRD region where $ClNO_2$ was less abundant during the simulated summer period (Figure 2d), the increases in RO_x and O_3 were much smaller.

In comparison, HONO, which is mostly concentrated within the near-surface layer, significantly affected the total RO_x and O_3 levels at the surface (Figure 6 and Figure S4), with enhancements of 2.8–4.6 ppt (28–37%) and 2.9–6.2 ppb (6–13%), respectively, in the daytime averages of RO_x and O_3 over the three most-developed regions. It had much smaller or even negative impacts above 300 m a.g.l. The simulated O_3 slightly decreased in some remote regions that were considered NO_x-limited regions (Figure 5f and Figure S4) because the heterogeneous formation of HONO (the major source of HONO)

would consume NO_2 and lead to less O_3 production in these NO_x-limited regions. As shown in Figures S1 and S2, the regional average of NO_2 decreased by 17% in the ReNOM case as compared with the base case over eastern China.

The combined effects of HONO and $ClNO_2$ on surface O_3 in the ReNOM case are illustrated in Figure 5c, which shows that O_3 was significantly enhanced by 8–10 ppb (10–15%) in the three developed regions, by 4–8 ppb in Hubei province in central China, and by 6–8 ppb in Sichuan province in southwestern China. On average, $ClNO_2$ and HONO increased the regional O_3 levels in the NCP, YRD, and PRD regions by 11.5%, 13.5%, and 13.3%, respectively, at the surface and by 7.8%, 7.1%, and 8.9% within the PBL, respectively (Figures 6j–6l). The simultaneous consideration of HONO and Cl-chemistry led to a larger O_3 enhancement compared to the summation of the effect of each chemistry (8.6% in the ReNOM case compared to 2.0% in the ReNOM_Cl case and 5.2% in the ReNOM_HONO case in daily O_3 enhancement over the whole domain). That is possibly because consideration of $N_2O_5/ClNO_2$ in the ReNOM case extended the cycling time of NO_x, and the photolysis of $ClNO_2$ released additional NO_2 during the day, which enhanced the heterogeneous formation of HONO (HONO increased by ~17% over eastern China in the ReNOM case compared to the ReNOM_HONO case; see Figure S5), amplifying the effects of HONO on the formation of O_3.

3.3.2 Improvement of O_3 predictions over China

In this section, we compare the simulated surface O_3 concentrations with observations during the simulation period to demonstrate the overall improvement of the revised WRF-Chem in simulating ground-level O_3. The results are shown in Table 5. There were 205, 141, and 67 monitoring stations available for the NCP, YRD, and PRD regions, respectively, and ~495 sites in other regions of China during the simulation period. It can be clearly seen that the default WRF-Chem model under-predicted the observed O_3 in the NCP and PRD regions by 9.9 ppb and 9.4 ppb, respectively, on average, whereas over-predicted the O_3 by 5.2 ppb at stations over the YRD region (also see Figure 7). The over-predictions over the YRD region were possibly due to overestimating the anthropogenic NO_x emission in the MEIC over this area. The uncertainties in the anthropogenic emissions (and other model inputs) would obviously affect the simulations of O_3 with WRF-Chem (Ahmadov et al., 2015). However, discussion on these uncertainties is beyond the scope of this study. Compared with the surface observations of NO_2 at the MEP's network, our model over-predicted the averaged NO_2 over the YRD region (see Figure S1 in the supplementary information). Over all of China (~908 sites), the default WRF-Chem model simulated daily O_3 of 31.0 ppb in the base case, compared with the observed value of 35.3 ppb.

When considering Cl-chemistry alone, the model noticeably improved the O_3 prediction over China by reducing the mean bias by 1.5 ppb (4.4%) in the ReNOM_Cl case. The inclusion of HONO (in the ReNOM_HONO case) alone provided a larger improvement in O_3 prediction, reducing the normalized mean bias (NMB) from -12.2% to -3.5%. By considering the two components in the new CBMZ_ReNOM module, the mean simulated O_3 concentrations at monitoring stations all over China increased from 31.0 ppb in the base case to 35.5 ppb in the ReNOM case, much closer to the averaged observations

and with significant decreases in mean bias (decreased from -4.3 ppb to 0.1 ppb) and NMB (reduced from -12.2% to 0.4%) and with a modest improvement in correlation between the simulated and observed O_3 levels (see Table 5). These results indicate a considerable improvement in the ability of the WRF-Chem model to simulate ground-level O_3 and possibly other secondary pollutants.

4 Summary and conclusions

In this study, we incorporated comprehensive processes of HONO and chlorine chemistry into a new chemical mechanism option, CBMZ_ReNOM, in the WRF-Chem model and applied the new model to simulating the spatial distribution of HONO, $ClNO_2$, and N_2O_5 and their impact on O_3 in China during a 12-day period in summer. Model simulations with the new module indicated that HONO was concentrated over the NCP, YRD, and PRD regions, with levels of 800−1800 ppt at ground-level, whereas the simulated N_2O_5 and $ClNO_2$ were most abundant within the 0–600 m layer, with average concentrations of 100–160 ppt and 800–1200 ppt, respectively, over the NCP, YRD, central China, and Sichuan Basin. The combined processes of HONO and chlorine chemistry increased RO_x mixing ratios by 36.3–44.7% at the surface and 4–37% within the PBL during the simulation period in summer and enhanced the daytime O_3 levels over the NCP, YRD, and PRD regions by 11.5–13.5% (2.9–6.5 ppb) at the surface and up to 10.9% in upper levels within the PBL. HONO had a more obvious impact on daytime O_3 at the surface and near-surface layer, whereas $ClNO_2$ showed significant influence above ~300 m a.g.l. over the NCP and YRD regions. With current emission estimates, we showed that the revised WRF-Chem model generally improved O_3 prediction across China. Our results suggest the importance of HONO and $ClNO_2$ in the formation of O_3 in the lower troposphere over polluted regions in China, and underscore the need for considering these reactive nitrogen species in chemical transport models to better predict ozone and other secondary pollutants.

Acknowledgements. The authors would like to thank the China Meteorological Administration for providing the meteorological observations and the China Ministry of Environmental Protection Ministry for the O_3 and NO_2 observations. This work was financially supported by the Hong Kong Research Grant Council (project C5022-14G and PolyU 153042/15E), the National Natural Science Foundation of China (41275123 and 91544213), and the Hong Kong Polytechnic University (1-ZE13). Both the data and source codes of the revised model used in this study are available from the authors upon request (cetwang@polyu.edu.hk).

References

Ahmadov, R., McKeen, S., Trainer, M., Banta, R., Brewer, A., Brown, S., Edwards, P. M., de Gouw, J. A., Frost, G. J., Gilman, J., Helmig, D., Johnson, B., Karion, A., Koss, A., Langford, A., Lerner, B., Olson, J., Oltmans, S., Peischl, J., Pétron, G., Pichugina, Y., Roberts, J. M., Ryerson, T., Schnell, R., Senff, C., Sweeney, C., Thompson, C., Veres, P. R., Warneke, C., Wild, R., Williams, E. J., Yuan, B., and Zamora, R.: Understanding high wintertime ozone pollution events in an oil- and natural gas-producing region of the western US, Atmos. Chem. Phys., 15, 411-429, 10.5194/acp-15-411-2015, 2015.

An, J., Li, Y., Chen, Y., Li, J., Qu, Y., and Tang, Y.: Enhancements of major aerosol components due to additional HONO sources in the North China Plain and implications for visibility and haze, Adv. Atmos. Sci., 30, 57-66, 10.1007/s00376-012-2016-9, 2013.

Archer-Nicholls, S., Lowe, D., Utembe, S., Allan, J., Zaveri, R. A., Fast, J. D., Hodnebrog, Ø., Denier van der Gon, H., and McFiggans, G.: Gaseous chemistry and aerosol mechanism developments for version 3.5.1 of the online regional model, WRF-Chem, Geosci. Model Dev., 7, 2557-2579, 10.5194/gmd-7-2557-2014, 2014.

Bertram, T. H., and Thornton, J. A.: Toward a general parameterization of N_2O_5 reactivity on aqueous particles: the competing effects of particle liquid water, nitrate and chloride, Atmos. Chem. Phys., 9, 8351-8363, 10.5194/acp-9-8351-2009, 2009.

Brown, S. S.: Variability in nocturnal nitrogen oxide processing and its role in regional air quality, Science, 311, 67-70, 2006.

Brown, S. S., Dubé, W. P., Tham, Y. J., Zha, Q., Xue, L., Poon, S., Wang, Z., Blake, D. R., Tsui, W., Parrish, D. D., and Wang, T.: Nighttime chemistry at a high altitude site above Hong Kong, J. Geophys. Res.-Atmos., 121, 2015JD024566, 10.1002/2015JD024566, 2016.

Chen, F., and Dudhia, J.: Coupling an Advanced Land Surface–Hydrology Model with the Penn State–NCAR MM5 Modeling System. Part I: Model Implementation and Sensitivity, Mon. Weather Rev., 129, 569-585, 10.1175/1520-0493(2001)129<0569:CAALSH>2.0.CO;2, 2001.

Chou, M.-D., Suarez, M. J., Ho, C.-H., Yan, M. M. H., and Lee, K.-T.: Parameterizations for Cloud Overlapping and Shortwave Single-Scattering Properties for Use in General Circulation and Cloud Ensemble Models, J. Clim., 11, 202-214, 10.1175/1520-0442(1998)011<0202:PFCOAS>2.0.CO;2, 1998.

Elshorbany, Y. F., Steil, B., Brühl, C., and Lelieveld, J.: Impact of HONO on global atmospheric chemistry calculated with an empirical parameterization in the EMAC model, Atmos. Chem. Phys., 12, 9977-10000, 10.5194/acp-12-9977-2012, 2012.

Emmons, L. K., Walters, S., Hess, P. G., Lamarque, J. F., Pfister, G. G., Fillmore, D., Granier, C., Guenther, A., Kinnison, D., Laepple, T., Orlando, J., Tie, X., Tyndall, G., Wiedinmyer, C., Baughcum, S. L., and Kloster, S.: Description and evaluation of the Model for Ozone and Related chemical Tracers, version 4 (MOZART-4), Geosci. Model Dev., 3, 43-67, 10.5194/gmd-3-43-2010, 2010.

Fast, J. D., Gustafson, W. I., Easter, R. C., Zaveri, R. A., Barnard, J. C., Chapman, E. G., Grell, G. A., and Peckham, S. E.: Evolution of ozone, particulates, and aerosol direct radiative forcing in the vicinity of Houston using a fully coupled meteorology-chemistry-aerosol model, J. Geophys. Res.-Atmos., 111, D21305, 10.1029/2005JD006721, 2006.

Fu, X., Wang, S., Zhao, B., Xing, J., Cheng, Z., Liu, H., and Hao, J.: Emission inventory of primary pollutants and chemical speciation in 2010 for the Yangtze River Delta region, China, Atmos. Environ., 70, 39-50, http://dx.doi.org/10.1016/j.atmosenv.2012.12.034, 2013.

Gonçalves, M., Dabdub, D., Chang, W. L., Jorba, O., and Baldasano, J. M.: Impact of HONO sources on the performance of mesoscale air quality models, Atmos. Environ., 54, 168-176, http://dx.doi.org/10.1016/j.atmosenv.2012.02.079, 2012.

Grell, G. A., and Dévényi, D.: A generalized approach to parameterizing convection combining ensemble and data assimilation techniques, Geophys. Res. Lett., 29, 38-31-38-34, 10.1029/2002GL015311, 2002.

Grell, G. A., Peckham, S. E., Schmitz, R., McKeen, S. A., Frost, G., Skamarock, W. C., and Eder, B.: Fully coupled "online" chemistry within the WRF model, Atmos. Environ., 39, 6957-6975, http://dx.doi.org/10.1016/j.atmosenv.2005.04.027, 2005.

Guenther, A., Karl, T., Harley, P., Wiedinmyer, C., Palmer, P. I., and Geron, C.: Estimates of global terrestrial isoprene emissions using MEGAN (Model of Emissions of Gases and Aerosols from Nature), Atmos. Chem. Phys., 6, 3181-3210,

10.5194/acp-6-3181-2006, 2006.

Hao, N., Zhou, B., Chen, D., and Chen, L.-m.: Observations of nitrous acid and its relative humidity dependence in Shanghai, J. Environ. Sci., 18, 910-915, http://dx.doi.org/10.1016/S1001-0742(06)60013-2, 2006.

Janjić, Z. I.: The Step-Mountain Eta Coordinate Model: Further Developments of the Convection, Viscous Sublayer, and Turbulence Closure Schemes, Mon. Weather Rev., 122, 927-945, 10.1175/1520-0493(1994)122<0927:tsmecm>2.0.co;2, 1994.

Kaiser, E. W., and Wu, C. H.: Measurement of the rate constant of the reaction of nitrous acid with nitric acid, The Journal of Physical Chemistry, 81, 187-190, 10.1021/j100518a001, 1977a.

Kaiser, E. W., and Wu, C. H.: A kinetic study of the gas phase formation and decomposition reactions of nitrous acid, The Journal of Physical Chemistry, 81, 1701-1706, 10.1021/j100533a001, 1977b.

Kanaya, Y., Cao, R., Akimoto, H., Fukuda, M., Komazaki, Y., Yokouchi, Y., Koike, M., Tanimoto, H., Takegawa, N., and Kondo, Y.: Urban photochemistry in central Tokyo: 1. Observed and modeled OH and HO_2 radical concentrations during the winter and summer of 2004, J. Geophys. Res.-Atmos., 112, D21312, 10.1029/2007JD008670, 2007.

Keene, W. C., Khalil, M. A. K., Erickson, D. J., McCulloch, A., Graedel, T. E., Lobert, J. M., Aucott, M. L., Gong, S. L., Harper, D. B., Kleiman, G., Midgley, P., Moore, R. M., Seuzaret, C., Sturges, W. T., Benkovitz, C. M., Koropalov, V., Barrie, L. A., and Li, Y. F.: Composite global emissions of reactive chlorine from anthropogenic and natural sources: Reactive Chlorine Emissions Inventory, J. Geophys. Res.-Atmos., 104, 8429-8440, 10.1029/1998JD100084, 1999.

Kim, S., Kim, S. Y., Lee, M., Shim, H., Wolfe, G. M., Guenther, A. B., He, A., Hong, Y., and Han, J.: Impact of isoprene and HONO chemistry on ozone and OVOC formation in a semirural South Korean forest, Atmos. Chem. Phys., 15, 4357-4371, 10.5194/acp-15-4357-2015, 2015.

Kleffmann, J.: Daytime Sources of Nitrous Acid (HONO) in the Atmospheric Boundary Layer, ChemPhysChem, 8, 1137-1144, 10.1002/cphc.200700016, 2007.

Kurtenbach, R., Becker, K. H., Gomes, J. A. G., Kleffmann, J., Lörzer, J. C., Spittler, M., Wiesen, P., Ackermann, R., Geyer, A., and Platt, U.: Investigations of emissions and heterogeneous formation of HONO in a road traffic tunnel, Atmos. Environ., 35, 3385-3394, http://dx.doi.org/10.1016/S1352-2310(01)00138-8, 2001.

Kusaka, H., Kondo, H., Kikegawa, Y., and Kimura, F.: A Simple Single-Layer Urban Canopy Model For Atmospheric Models: Comparison With Multi-Layer And Slab Models, Bound. Layer Meteorol., 101, 329-358, 10.1023/A:1019207923078, 2001.

Lei, Y., Zhang, Q., He, K. B., and Streets, D. G.: Primary anthropogenic aerosol emission trends for China, 1990–2005, Atmos. Chem. Phys., 11, 931-954, 10.5194/acp-11-931-2011, 2011.

Li, G., Lei, W., Zavala, M., Volkamer, R., Dusanter, S., Stevens, P., and Molina, L. T.: Impacts of HONO sources on the photochemistry in Mexico City during the MCMA-2006/MILAGO Campaign, Atmos. Chem. Phys., 10, 6551-6567, 10.5194/acp-10-6551-2010, 2010.

Li, M., Zhang, Q., Kurokawa, J. I., Woo, J. H., He, K., Lu, Z., Ohara, T., Song, Y., Streets, D. G., Carmichael, G. R., Cheng, Y., Hong, C., Huo, H., Jiang, X., Kang, S., Liu, F., Su, H., and Zheng, B.: MIX: a mosaic Asian anthropogenic emission inventory under the international collaboration framework of the MICS-Asia and HTAP, Atmos. Chem. Phys., 17, 935-963, 10.5194/acp-17-935-2017, 2017.

Li, Q., Zhang, L., Wang, T., Tham, Y. J., Ahmadov, R., Xue, L., Zhang, Q., and Zheng, J.: Impacts of heterogeneous uptake of dinitrogen pentoxide and chlorine activation on ozone and reactive nitrogen partitioning: improvement and application of the WRF-Chem model in southern China, Atmos. Chem. Phys., 16, 14875-14890, 10.5194/acp-16-14875-2016, 2016.

Li, X., Brauers, T., Häseler, R., Bohn, B., Fuchs, H., Hofzumahaus, A., Holland, F., Lou, S., Lu, K. D., Rohrer, F., Hu, M., Zeng, L. M., Zhang, Y. H., Garland, R. M., Su, H., Nowak, A., Wiedensohler, A., Takegawa, N., Shao, M., and Wahner, A.: Exploring the atmospheric chemistry of nitrous acid (HONO) at a rural site in Southern China, Atmos. Chem. Phys., 12, 1497-1513, 10.5194/acp-12-1497-2012, 2012.

Li, Y., An, J., Min, M., Zhang, W., Wang, F., and Xie, P.: Impacts of HONO sources on the air quality in Beijing, Tianjin and Hebei Province of China, Atmos. Environ., 45, 4735-4744, http://dx.doi.org/10.1016/j.atmosenv.2011.04.086, 2011.

Lin, Y.-C., Cheng, M.-T., Ting, W.-Y., and Yeh, C.-R.: Characteristics of gaseous HNO_2, HNO_3, NH_3 and particulate ammonium nitrate in an urban city of Central Taiwan, Atmos. Environ., 40, 4725-4733, http://dx.doi.org/10.1016/j.atmosenv.2006.04.037, 2006.

Lin, Y.-L., Farley, R. D., and Orville, H. D.: Bulk Parameterization of the Snow Field in a Cloud Model, J. Clim. Appl. Meteorol., 22, 1065-1092, 10.1175/1520-0450(1983)022<1065:BPOTSF>2.0.CO;2, 1983.

Lowe, D., Archer-Nicholls, S., Morgan, W., Allan, J., Utembe, S., Ouyang, B., Aruffo, E., Le Breton, M., Zaveri, R. A., Di Carlo, P., Percival, C., Coe, H., Jones, R., and McFiggans, G.: WRF-Chem model predictions of the regional impacts of N_2O_5 heterogeneous processes on night-time chemistry over north-western Europe, Atmos. Chem. Phys., 15, 1385-1409, 10.5194/acp-15-1385-2015, 2015.

Madronich, S.: Photodissociation in the atmosphere: 1. Actinic flux and the effects of ground reflections and clouds, J. Geophys. Res.-Atmos., 92, 9740-9752, 10.1029/JD092iD08p09740, 1987.

Mlawer, E. J., Taubman, S. J., Brown, P. D., Iacono, M. J., and Clough, S. A.: Radiative transfer for inhomogeneous atmospheres: RRTM, a validated correlated-k model for the longwave, J. Geophys. Res.: Atmospheres, 102, 16663-16682, 10.1029/97JD00237, 1997a.

Mlawer, E. J., Taubman, S. J., Brown, P. D., Iacono, M. J., and Clough, S. A.: Radiative transfer for inhomogeneous atmospheres: RRTM, a validated correlated-k model for the longwave, J. Geophys. Res.-Atmos., 102, 16663-16682, 10.1029/97JD00237, 1997b.

Nakayama, T., Ide, T., Taketani, F., Kawai, M., Takahashi, K., and Matsumi, Y.: Nighttime measurements of ambient N_2O_5, NO_2, NO and O_3 in a sub-urban area, Toyokawa, Japan, Atmos. Environ., 42, 1995-2006, http://dx.doi.org/10.1016/j.atmosenv.2007.12.001, 2008.

Noguchi, I., Hayashi, K., Kato, T., Yamaguchi, T., Akiyama, M., Otsuka, H., Sakai, S., Takagi, K., Fukazawa, T., Shibata, H., Fujinuma, Y., Saigusa, N., Shimotori, M., Endo, T., Yago, H., Matsuda, K., Tsunogai, U., and Hara, H.: Atmospheric Behavior of Nitrous Acid and Nitrogen Dioxide in Northern Japan, Journal of Japan Society for Atmospheric Environment / Taiki Kankyo Gakkaishi, 45, 153-165, 10.11298/taiki.45.153, 2010.

Osthoff, H. D., Roberts, J. M., Ravishankara, A. R., Williams, E. J., Lerner, B. M., Sommariva, R., Bates, T. S., Coffman, D., Quinn, P. K., Dibb, J. E., Stark, H., Burkholder, J. B., Talukdar, R. K., Meagher, J., Fehsenfeld, F. C., and Brown, S. S.: High levels of nitryl chloride in the polluted subtropical marine boundary layer, Nature Geosci, 1, 324-328, http://www.nature.com/ngeo/journal/v1/n5/suppinfo/ngeo177_S1.html, 2008.

Oswald, R., Behrendt, T., Ermel, M., Wu, D., Su, H., Cheng, Y., Breuninger, C., Moravek, A., Mougin, E., Delon, C., Loubet, B., Pommerening-Röser, A., Sörgel, M., Pöschl, U., Hoffmann, T., Andreae, M. O., Meixner, F. X., and Trebs, I.: HONO Emissions from Soil Bacteria as a Major Source of Atmospheric Reactive Nitrogen, Science, 341, 1233-1235, 10.1126/science.1242266, 2013.

Qin, M., Xie, P., Su, H., Gu, J., Peng, F., Li, S., Zeng, L., Liu, J., Liu, W., and Zhang, Y.: An observational study of the HONO–NO_2 coupling at an urban site in Guangzhou City, South China, Atmos. Environ., 43, 5731-5742, http://dx.doi.org/10.1016/j.atmosenv.2009.08.017, 2009.

Riemer, N., Vogel, H., Vogel, B., Anttila, T., Kiendler-Scharr, A., and Mentel, T. F.: Relative importance of organic coatings for the heterogeneous hydrolysis of N_2O_5 during summer in Europe, J. Geophys. Res.-Atmos., 114, D17307, 10.1029/2008JD011369, 2009.

Rivera-Figueroa, A. M., Sumner, A. L., and Finlayson-Pitts, B. J.: Laboratory Studies of Potential Mechanisms of Renoxification of Tropospheric Nitric Acid, Environ. Sci. Technol., 37, 548-554, 10.1021/es020828g, 2003.

Roberts, J. M., Osthoff, H. D., Brown, S. S., and Ravishankara, A. R.: N_2O_5 Oxidizes Chloride to Cl_2 in Acidic Atmospheric Aerosol, Science, 321, 1059-1059, 10.1126/science.1158777, 2008.

Roberts, J. M., Osthoff, H. D., Brown, S. S., Ravishankara, A. R., Coffman, D., Quinn, P., and Bates, T.: Laboratory studies of products of N_2O_5 uptake on Cl^- containing substrates, Geophys. Res. Lett., 36, L20808, 10.1029/2009GL040448, 2009.

Sarwar, G., Roselle, S. J., Mathur, R., Appel, W., Dennis, R. L., and Vogel, B.: A comparison of CMAQ HONO predictions with observations from the Northeast Oxidant and Particle Study, Atmos. Environ., 42, 5760-5770, http://dx.doi.org/10.1016/j.atmosenv.2007.12.065, 2008.

Sarwar, G., Simon, H., Bhave, P., and Yarwood, G.: Examining the impact of heterogeneous nitryl chloride production on air quality across the United States, Atmos. Chem. Phys., 12, 6455-6473, 10.5194/acp-12-6455-2012, 2012.

Sarwar, G., Simon, H., Xing, J., and Mathur, R.: Importance of tropospheric $ClNO_2$ chemistry across the Northern Hemisphere, Geophys. Res. Lett., 41, 2014GL059962, 10.1002/2014GL059962, 2014.

Simon, H., Kimura, Y., McGaughey, G., Allen, D. T., Brown, S. S., Coffman, D., Dibb, J., Osthoff, H. D., Quinn, P., Roberts,

J. M., Yarwood, G., Kemball-Cook, S., Byun, D., and Lee, D.: Modeling heterogeneous ClNO₂ formation, chloride availability, and chlorine cycling in Southeast Texas, Atmos. Environ., 44, 5476-5488, http://dx.doi.org/10.1016/j.atmosenv.2009.09.006, 2010.

Smith, J. D., DeSain, J. D., and Taatjes, C. A.: Infrared laser absorption measurements of HCl(v=1) production in reactions of Cl atoms with isobutane, methanol, acetaldehyde, and toluene at 295 K, Chem. Phys. Lett., 366, 417-425, http://doi.org/10.1016/S0009-2614(02)01621-4, 2002.

Song, C. H., Park, M. E., Lee, E. J., Lee, J. H., Lee, B. K., Lee, D. S., Kim, J., Han, J. S., Moon, K. J., and Kondo, Y.: Possible particulate nitrite formation and its atmospheric implications inferred from the observations in Seoul, Korea, Atmos. Environ., 43, 2168-2173, http://dx.doi.org/10.1016/j.atmosenv.2009.01.018, 2009.

Spataro, F., Ianniello, A., Esposito, G., Allegrini, I., Zhu, T., and Hu, M.: Occurrence of atmospheric nitrous acid in the urban area of Beijing (China), Sci. Total Environ., 447, 210-224, http://dx.doi.org/10.1016/j.scitotenv.2012.12.065, 2013.

Su, H., Cheng, Y. F., Shao, M., Gao, D. F., Yu, Z. Y., Zeng, L. M., Slanina, J., Zhang, Y. H., and Wiedensohler, A.: Nitrous acid (HONO) and its daytime sources at a rural site during the 2004 PRIDE-PRD experiment in China, J. Geophys. Res.-Atmos., 113, D14312, 10.1029/2007JD009060, 2008.

Su, H., Cheng, Y., Oswald, R., Behrendt, T., Trebs, I., Meixner, F. X., Andreae, M. O., Cheng, P., Zhang, Y., and Pöschl, U.: Soil Nitrite as a Source of Atmospheric HONO and OH Radicals, Science, 333, 1616-1618, 10.1126/science.1207687, 2011.

Takeuchi, M., Miyazaki, Y., Tsunoda, H., and Tanaka, H.: Atmospheric Acid Gases in Tokushima, Japan, Monitored with Parallel Plate Wet Denuder Coupled Ion Chromatograph, Analytical Sciences, 29, 165-168, 10.2116/analsci.29.165, 2013.

Tan, Z., Fuchs, H., Lu, K., Hofzumahaus, A., Bohn, B., Broch, S., Dong, H., Gomm, S., Häseler, R., He, L., Holland, F., Li, X., Liu, Y., Lu, S., Rohrer, F., Shao, M., Wang, B., Wang, M., Wu, Y., Zeng, L., Zhang, Y., Wahner, A., and Zhang, Y.: Radical chemistry at a rural site (Wangdu) in the North China Plain: observation and model calculations of OH, HO₂ and RO₂ radicals, Atmos. Chem. Phys., 17, 663-690, 10.5194/acp-17-663-2017, 2017.

Tanaka, P. L., Allen, D. T., McDonald-Buller, E. C., Chang, S., Kimura, Y., Mullins, C. B., Yarwood, G., and Neece, J. D.: Development of a chlorine mechanism for use in the carbon bond IV chemistry model, J. Geophys. Res.-Atmos., 108, 4145, 10.1029/2002JD002432, 2003.

Tang, Y., An, J., Wang, F., Li, Y., Qu, Y., Chen, Y., and Lin, J.: Impacts of an unknown daytime HONO source on the mixing ratio and budget of HONO, and hydroxyl, hydroperoxyl, and organic peroxy radicals, in the coastal regions of China, Atmos. Chem. Phys., 15, 9381-9398, 10.5194/acp-15-9381-2015, 2015.

Tham, Y. J., Wang, Z., Li, Q., Yun, H., Wang, W., Wang, X., Xue, L., Lu, K., Ma, N., Bohn, B., Li, X., Kecorius, S., Groß, J., Shao, M., Wiedensohler, A., Zhang, Y., and Wang, T.: Significant concentrations of nitryl chloride sustained in the morning: investigations of the causes and impacts on ozone production in a polluted region of northern China, Atmos. Chem. Phys., 16, 14959-14977, 10.5194/acp-16-14959-2016, 2016.

Thornton, J. A., Kercher, J. P., Riedel, T. P., Wagner, N. L., Cozic, J., Holloway, J. S., Dubé, W. P., Wolfe, G. M., Quinn, P. K., Middlebrook, A. M., Alexander, B., and Brown, S. S.: A large atomic chlorine source inferred from mid-continental reactive nitrogen chemistry, Nature, 464, 271-274, http://www.nature.com/nature/journal/v464/n7286/suppinfo/nature08905_S1.html, 2010.

Tsai, J.-H., Chang, L.-P., and Chiang, H.-L.: Airborne pollutant characteristics in an urban, industrial and agricultural complex metroplex with high emission loading and ammonia concentration, Sci. Total Environ., 494–495, 74-83, http://dx.doi.org/10.1016/j.scitotenv.2014.06.120, 2014.

Wallington, T. J., Skewes, L. M., and Siegl, W. O.: Kinetics of the gas phase reaction of chlorine atoms with a series of alkenes, alkynes and aromatic species at 295 K, J. Photochem. Photobiol. A, 45, 167-175, http://dx.doi.org/10.1016/1010-6030(88)80126-6, 1988.

Wang, T., Wei, X. L., Ding, A. J., Poon, C. N., Lam, K. S., Li, Y. S., Chan, L. Y., and Anson, M.: Increasing surface ozone concentrations in the background atmosphere of Southern China, 1994–2007, Atmos. Chem. Phys., 9, 6217-6227, 10.5194/acp-9-6217-2009, 2009.

Wang, T., Tham, Y. J., Xue, L., Li, Q., Zha, Q., Wang, Z., Poon, S. C. N., Dubé, W. P., Blake, D. R., Louie, P. K. K., Luk, C. W. Y., Tsui, W., and Brown, S. S.: Observations of nitryl chloride and modeling its source and effect on ozone in the planetary boundary layer of southern China, J. Geophys. Res.-Atmos., 121, 2015JD024556, 10.1002/2015JD024556,

2016.

Wang, T., Xue, L., Brimblecombe, P., Lam, Y. F., Li, L., and Zhang, L.: Ozone pollution in China: A review of concentrations, meteorological influences, chemical precursors, and effects, Sci. Total Environ., 575, 1582-1596, http://doi.org/10.1016/j.scitotenv.2016.10.081, 2017.

5   Wild, O., Zhu, X., and Prather, M. J.: Fast-J: Accurate Simulation of In- and Below-Cloud Photolysis in Tropospheric Chemical Models, J. Atmos. Chem., 37, 245-282, 10.1023/a:1006415919030, 2000.

Xu, Z., Wang, T., Xue, L. K., Louie, P. K. K., Luk, C. W. Y., Gao, J., Wang, S. L., Chai, F. H., and Wang, W. X.: Evaluating the uncertainties of thermal catalytic conversion in measuring atmospheric nitrogen dioxide at four differently polluted sites in China, Atmos. Environ., 76, 221-226, http://doi.org/10.1016/j.atmosenv.2012.09.043, 2013.

10   Yang, Q., Su, H., Li, X., Cheng, Y., Lu, K., Cheng, P., Gu, J., Guo, S., Hu, M., Zeng, L., Zhu, T., and Zhang, Y.: Daytime HONO formation in the suburban area of the megacity Beijing, China, Sci. China Chem., 57, 1032-1042, 10.1007/s11426-013-5044-0, 2014.

Zaveri, R. A., and Peters, L. K.: A new lumped structure photochemical mechanism for large-scale applications, J. Geophys. Res.-Atmos., 104, 30387-30415, 10.1029/1999JD900876, 1999.

15   Zaveri, R. A., Easter, R. C., Fast, J. D., and Peters, L. K.: Model for Simulating Aerosol Interactions and Chemistry (MOSAIC), J. Geophys. Res.-Atmos., 113, D13204, 10.1029/2007JD008782, 2008.

Zha, Q., Xue, L., Wang, T., Xu, Z., Yeung, C., Louie, P. K. K., and Luk, C. W. Y.: Large conversion rates of NO_2 to HNO_2 observed in air masses from the South China Sea: Evidence of strong production at sea surface?, Geophys. Res. Lett., 41, 2014GL061429, 10.1002/2014GL061429, 2014.

20   Zhang, L., Wang, T., Lv, M., and Zhang, Q.: On the severe haze in Beijing during January 2013: Unraveling the effects of meteorological anomalies with WRF-Chem, Atmos. Environ., 104, 11-21, http://dx.doi.org/10.1016/j.atmosenv.2015.01.001, 2015.

Zhang, L., Wang, T., Zhang, Q., Zheng, J., Xu, Z., and Lv, M.: Potential sources of nitrous acid (HONO) and their impacts on ozone: A WRF-Chem study in a polluted subtropical region, J. Geophys. Res.-Atmos., 121, 2015JD024468, 25   10.1002/2015JD024468, 2016.

Zhang, Q., Streets, D. G., Carmichael, G. R., He, K. B., Huo, H., Kannari, A., Klimont, Z., Park, I. S., Reddy, S., Fu, J. S., Chen, D., Duan, L., Lei, Y., Wang, L. T., and Yao, Z. L.: Asian emissions in 2006 for the NASA INTEX-B mission, Atmos. Chem. Phys., 9, 5131-5153, 10.5194/acp-9-5131-2009, 2009.

Zhou, X., Zhang, N., TerAvest, M., Tang, D., Hou, J., Bertman, S., Alaghmand, M., Shepson, P. B., Carroll, M. A., Griffith, 30   S., Dusanter, S., and Stevens, P. S.: Nitric acid photolysis on forest canopy surface as a source for tropospheric nitrous acid, Nature Geosci, 4, 440-443, 2011.

35

40

Table 1. Mechanism of chlorine chemistry in the CBMZ_ReNOM in WRF-Chem.

No.	Reaction	Reaction rate[f]	Ref
01	$Cl_2 + hv \rightarrow Cl + Cl$	J_{Cl_2}	a
02	$HOCl + hv \rightarrow Cl + OH$	J_{HOCl}	a
03	$ClNO_2 + hv \rightarrow Cl + NO_2$	J_{ClNO_2}	a
04	$ClONO_2 + hv \rightarrow Cl + NO_3$	$0.83 \times J_{ClONO_2}$	a,b
05	$ClONO_2 + hv \rightarrow ClO + NO_2$	$0.17 \times J_{ClONO_2}$	a,b
06	$FMCl + hv \rightarrow Cl + CO + HO_2$	J_{FMCl}	a
07	$FMCl + OH \rightarrow Cl + CO + H_2O$	5.0×10^{-13}	a
08	$HCl + OH \rightarrow Cl + H_2O$	$ARRH(1.7 \times 10^{-12}, -230.0)$	a
09	$Cl_2 + OH \rightarrow HOCl + Cl$	$ARRH(3.6 \times 10^{-12}, -1200.0)$	a
10	$HOCl + OH \rightarrow ClO + H_2O$	5.0×10^{-13}	a
11	$ClO + ClO \rightarrow 0.3\ Cl_2 + 1.4\ Cl + O_2$	1.63×10^{-14}	a
12	$ClO + NO_2 \rightarrow ClONO_2$	7.0×10^{-11}	a
13	$ClO + NO \rightarrow Cl + NO_2$	$ARRH(6.4 \times 10^{-12}, 290.0)$	a
14	$ClO + HO_2 \rightarrow HOCl + O_2$	$ARRH(2.7 \times 10^{-12}, 220.0)$	a
15	$ClO + OH \rightarrow HO_2 + Cl$	1.8×10^{-11}	a
16	$ClO + OH \rightarrow HCl + O_2$	1.2×10^{-12}	a
17	$Cl + O_3 \rightarrow ClO + O_2$	$ARRH(2.3 \times 10^{-11}, -200.0)$	a
18	$Cl + NO_2 \rightarrow ClNO_2$	$TROE(1.8 \times 10^{-31}, 2.0, 1.0 \times 10^{-10}, 1.0)$	c
19	$Cl + HO_2 \rightarrow HCl + O_2$	3.5×10^{-11}	a
20	$Cl + HO_2 \rightarrow ClO + OH$	$ARRH(7.5 \times 10^{-11}, -620.0)$	a
21	$Cl + H_2O_2 \rightarrow HCl + HO_2$	$ARRH(1.1 \times 10^{-11}, -980.0)$	a
22	$Cl + NO_3 \rightarrow NO_2 + ClO$	2.4×10^{-11}	a
23	$Cl + ClONO_2 \rightarrow Cl_2 + NO_3$	$ARRH(6.2 \times 10^{-12}, 145.0)$	a
24	$Cl + CH_4 \rightarrow HCl + CH_3O_2$	$ARRH(6.6 \times 10^{-12}, -1240.0)$	a
25	$Cl + C_2H_6 \rightarrow HCl + 0.991\ ALD2 + XO_2 + HO_2$	$ARRH(8.3 \times 10^{-11}, -100.0)$	a
26	$Cl + PAR \rightarrow HCl + XO_2 + 0.11\ HO_2$ $+ 0.06\ ALD2 + 0.11\ PAR + 0.76\ RO_2$	5.0×10^{-11}	a
27	$Cl + ETH \rightarrow FMCl + 2\ XO_2 + HO_2 + HCHO$	1.07×10^{-10}	a
28	$Cl + OLE \rightarrow FMCl + 0.33\ ALD2 + 2\ XO_2 + HO_2 +$	2.5×10^{-10}	a

	PAR		
29	Cl + OLI → 0.3 HCl + 0.7 FMCl + 0.45 ALD2 + 0.3 OLE + 0.3 PAR + 1.7 XO2 + HO2	3.5×10^{-10}	a
30	Cl + ISOP → 0.15 HCl + XO2 + HO2 + 0.85 FMCl + ISOPRD	4.3×10^{-10}	a
31	Cl + HCHO → HCl + HO2 + CO	ARRH(8.2×10^{-11}, -34.0)	a
32	Cl + ALD2 → HCl + C2O3	7.9×10^{-11}	a
33	Cl + CH3OH → HCl + HO2 + HCHO	5.5×10^{-11}	a
34	Cl + ANOL → HCl + HO2 + ALD2	ARRH(8.2×10^{-11}, 45.0)	a
35	Cl + TOL → HCl + 0.88 XO2 + 0.88 HO2 + 0.12 NAP	6.1×10^{-11}	d
36	Cl + XYL → HCl + 0.84 XO2 + 0.84 HO2 + 0.16 NAP	1.2×10^{-10}	e

[a] The kinetic data are taken from the IUPAC database (http://iupac.pole-ether.fr/index.html); [b] The branching ratio is determined based on Tropospheric Ultraviolet Visible (TUV) Radiation model calculations; [c] Tanaka et al. (2003); [d] Smith et al. (2002); [e] Wallington et al. (1988); [f] The units for first order rate constants are s^{-1}; and for second order rate constants, cm^3 molecule^{-1} s^{-1}.

$$\text{ARRH}(\alpha, \beta) = \alpha \times \text{EXP}\left(-\frac{\beta}{T}\right); \ \text{TROE}(k_0^{300}, n, k_\infty^{300}, m) = \left(\frac{k_0(T)[M]}{1+\frac{k_0(T)[M]}{k_\infty(T)}}\right) \times 0.6^{\left\{1+\left[\log_{10}\left(\frac{k_0(T)[M]}{k_\infty(T)}\right)\right]^2\right\}^{-1}}, \ \text{where} \ k_0(T) = k_0^{300} \times \left(\frac{T}{300}\right)^{-n}; \ k_\infty(T) =$$

5    $k_\infty^{300} \times \left(\frac{T}{300}\right)^{-m}$; M is the number density; and T is the absolute temperature.

Cl2: molecular chlorine; Cl: atomic chlorine; HOCl: hypochlorous acid; ClNO2: nitryl chloride; ClONO2: chlorine nitrate; ClO: chlorine oxide; FMCl: formyl chloride; HCl: hydrochloric acid; NO: nitric oxide; NO2: nitrogen dioxide, NO3: nitrate radical; OH: hydroxyl radical; H2O: water vapor; HO2: hydroperoxy radical; H2O2: hydrogen peroxide; RO2: peroxy radical; O2: oxygen; O3: ozone; CO: carbon monoxide, CH4: methane; CH3O2: methylperoxy radical; C2H6: ethane; ALD2: acetaldehyde; XO2: NO to NO2 operator, PAR: paraffin
10   carbon; ETH: ethene; HCHO: formaldehyde; OLE: terminal olefinic carbons; OLI: internal olefinic carbons; ISOP: isoprene; ISOPRD: lumped intermediate; C2O3: peroxyacyl radical; CH3OH: methanol; ANOL: ethanol; TOL: toluene; NAP: nitratoalkyl peroxy radicals; XYL: xylene.

Table 2. WRF-Chem module configurations.

Major Modules	Option	Reference
Microphysics scheme	Lin	*Lin et al. (1983)*
Cumulus scheme	Grell and Dévényi	*Grell and Dévényi (2002)*
Longwave radiation	RRTM	*Mlawer et al. (1997b)*
Shortwave radiation	Goddard shortwave	*Chou et al. (1998)*
Land-surface physics	Noah LSM	*Chen and Dudhia (2001)*
Urban surface scheme	UCM	*Kusaka et al. (2001)*
PBL scheme	MYJ	*Janjić (1994)*
Photolysis scheme	Fast-J	*Fast et al. (2006)*
Chemical mechanism	CBMZ/CBMZ_ReNOM	*Zaveri and Peters (1999)*
Aerosol module	MOSAIC	*Zaveri et al. (2008); Archer-Nicholls et al. (2014)*

Table 3. Simulation cases of WRF-Chem model.

Case	Chemical Mechanism	HONO Chemistry	ClNO$_2$ Chemistry
BASE	CBMZ	None	None
ReNOM_Cl	CBMZ_ReNOM	None	Yes
ReNOM_HONO	CBMZ_ReNOM	Yes	None
ReNOM	CBMZ_ReNOM	Yes	Yes

Table 4. Comparisons between simulated and observed HONO (ppb), N_2O_5 (ppt), and $ClNO_2$ (ppt) over Asia from previous studies.

Species	Location	Observation Period	Observation average	Simulation average	Reference
HONO	Wangdu, NCP[a]	Jun-Jul 2014	0.94	0.81	Tan et al. (2017)
	Beijing (PKU), NCP[a]	Aug 2007	1.47	2.03	Spataro et al. (2013)
	Beijing (Yufa), NCP[a]	Aug 2006	0.76	1.07	Yang et al. (2014)
	Shanghai, YRD[a]	Oct-Jan 2004/05	1.10	1.15	Hao et al. (2006)
	Hong Kong (TC), PRD[a]	Aug 2011	0.92	0.78	Zhang et al. (2016)
	Xinken, PRD[a]	Oct-Nov 2004	1.20	0.18	Su et al. (2008)
	Guangzhou, PRD[a]	Jul 2006	2.80	1.49	Qin et al. (2009)
	Backgarden, PRD[a]	Jul 2006	0.59	0.83	Li et al. (2012)
	Taehwa, Korea	Jun 2012	0.60	2.26	Kim et al. (2015)
	Seoul, Korea	May-Jul 2005	0.36 (max 8.6)	2.75 (max 8.7)	Song et al. (2009)
	Tokyo, Japan	Jan-Feb 2004	0.43	0.45	Kanaya et al. (2007)
	Tokushima, Japan	Aug 2011	0.63	0.53	Takeuchi et al. (2013)
	Tokushima, Japan	Feb 2011	0.56	0.53	Takeuchi et al. (2013)
	Sapporo, Japan	Oct 2002	0.98	0.47	Noguchi et al. (2010)
	Kaohsiung, Taiwan	2005-2007 (multiple months)	2.13	2.58	Tsai et al. (2014)
	Taichung, Taiwan	Jan-Dec 2002	1.53	2.23	Lin et al. (2006)
N_2O_5	Wangdu, NCP[a]	Jun-Jul 2014	28.0	23.9	Tham et al. (2016)
	Mt. Tai, NCP[a]	Jul-Aug 2014	7.00	18.3	*unpublished data*
	Jinan, NCP[a]	Aug-Sep 2014	17.0	13.1	*unpublished data*
	Hong Kong (TMS), PRD[a]	Nov-Dec 2013	277.8 (nighttime)	6.27 (nighttime)	Wang et al. (2016)
	Toyokawa, Japan	Feb 2006	20.0 (max)	14.1 (max)	Nakayama et al. (2008)
$ClNO_2$	Wangdu, NCP[a]	Jun-Jul 2014	159.5	265.6	Tham et al. (2016)

Mt. Tai, NCP[a]	Jul-Aug 2014	30.4	117.4	*unpublished data*
Jinan, NCP[a]	Aug-Sep 2014	94.0	254.0	*unpublished data*
Hong Kong (TMS), PRD[a]	Nov-Dec 2013	74.6 (nighttime)	8.69 (nighttime)	Wang et al. (2016)

[a] NCP: Northern China Plain; YRD: Yangtze River Delta; PRD: Pearl River Delta; PKU: Peking University; TC: Tung Chung; TMS: Tai Mo Shan.

Table 5. Statistics of model performance in the base and ReNOM cases for hourly O$_3$ measurements (ppb) at ~908 MEP air quality monitoring stations during the simulation period (27 Jun-7 Jul 2014).

Region	Case	No. OBS[b]	OBS[b]	MOD[b]	COR[b]	MB[b]	RMSE[b]	NMB[b]	NME[b]
NCP[a]	BASE	49789	47.2	37.3	0.60	-9.9	26.8	-20.9%	44.0%
	ReNOM_Cl			40.0	0.61	-7.2	26.7	-15.3%	43.7%
	ReNOM_HONO			41.2	0.61	-6.0	26.4	-12.7%	43.3%
	ReNOM			43.5	0.61	-3.6	26.5	-7.7%	43.5%
YRD[a]	BASE	34857	31.5	36.8	0.56	5.2	29.3	16.6%	68.2%
	ReNOM_Cl			39.4	0.56	7.9	31.9	25.1%	72.7%
	ReNOM_HONO			43.3	0.54	11.8	34.3	37.3%	77.5%
	ReNOM			45.3	0.54	13.8	36.3	43.8%	81.7%
PRD[a]	BASE	15627	25.0	15.6	0.53	-9.4	28.0	-37.6%	75.8%
	ReNOM_Cl			15.6	0.53	-9.4	27.9	-37.6%	75.8%
	ReNOM_HONO			18.5	0.54	-6.4	26.3	-25.8%	73.7%
	ReNOM			18.4	0.54	-6.5	26.3	-26.1%	73.9%
China	BASE	214596	35.3	31.0	0.51	-4.3	27.3	-12.2%	57.5%
	ReNOM_Cl			32.6	0.51	-2.8	28.0	-7.8%	58.5%
	ReNOM_HONO			34.1	0.52	-1.2	26.7	-3.5%	56.6%
	ReNOM			35.5	0.52	0.1	26.1	0.4%	55.8%

[a] NCP: Northern China Plain; YRD: Yangtze River Delta; PRD: Pearl River Delta. [b] No. Obs: number of available observations used in evaluation; OBS: average observed value; MOD: average modeled value; COR: correlation; MB: mean bias; RMSE: root mean square error; NMB: normalized mean bias; NME: normalized mean error.
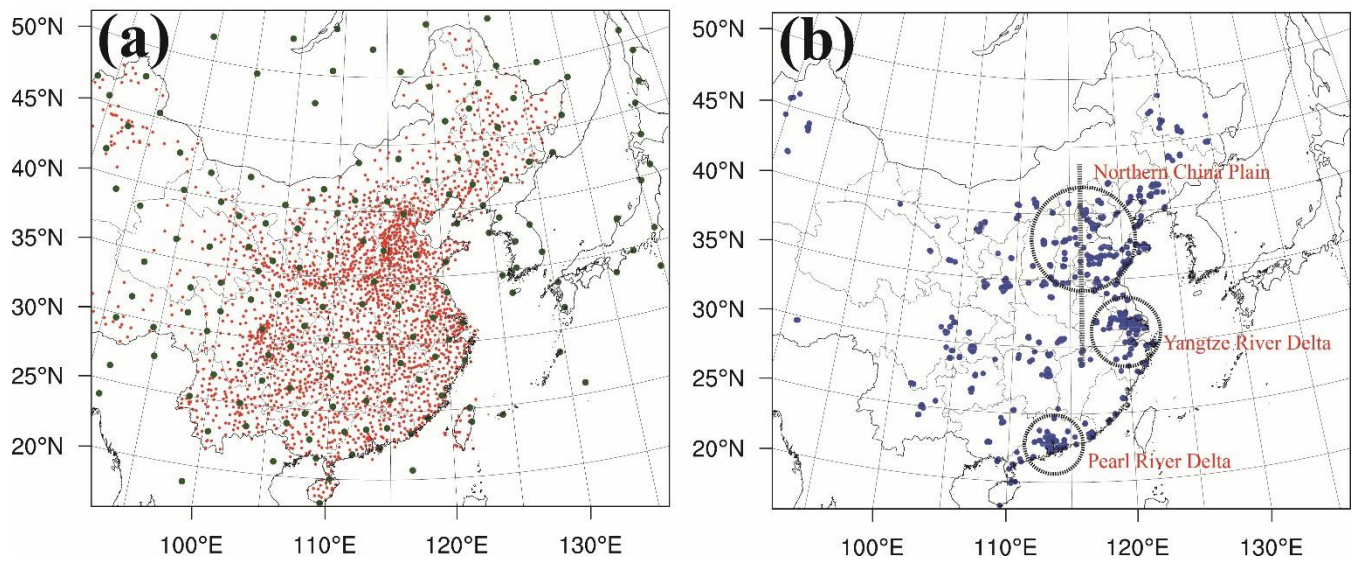
Figure 1. WRF-Chem domain used in this study. (a) Red dots denote the surface weather stations used in FDDA (tri-hourly); green dots are the sounding sites (12-hourly). (b) Blue dots denote the available surface air-quality monitoring stations operated by China MEP in 2014, and the dashed line represents the vertical domain that intercepts the most polluted Northern China Plain.
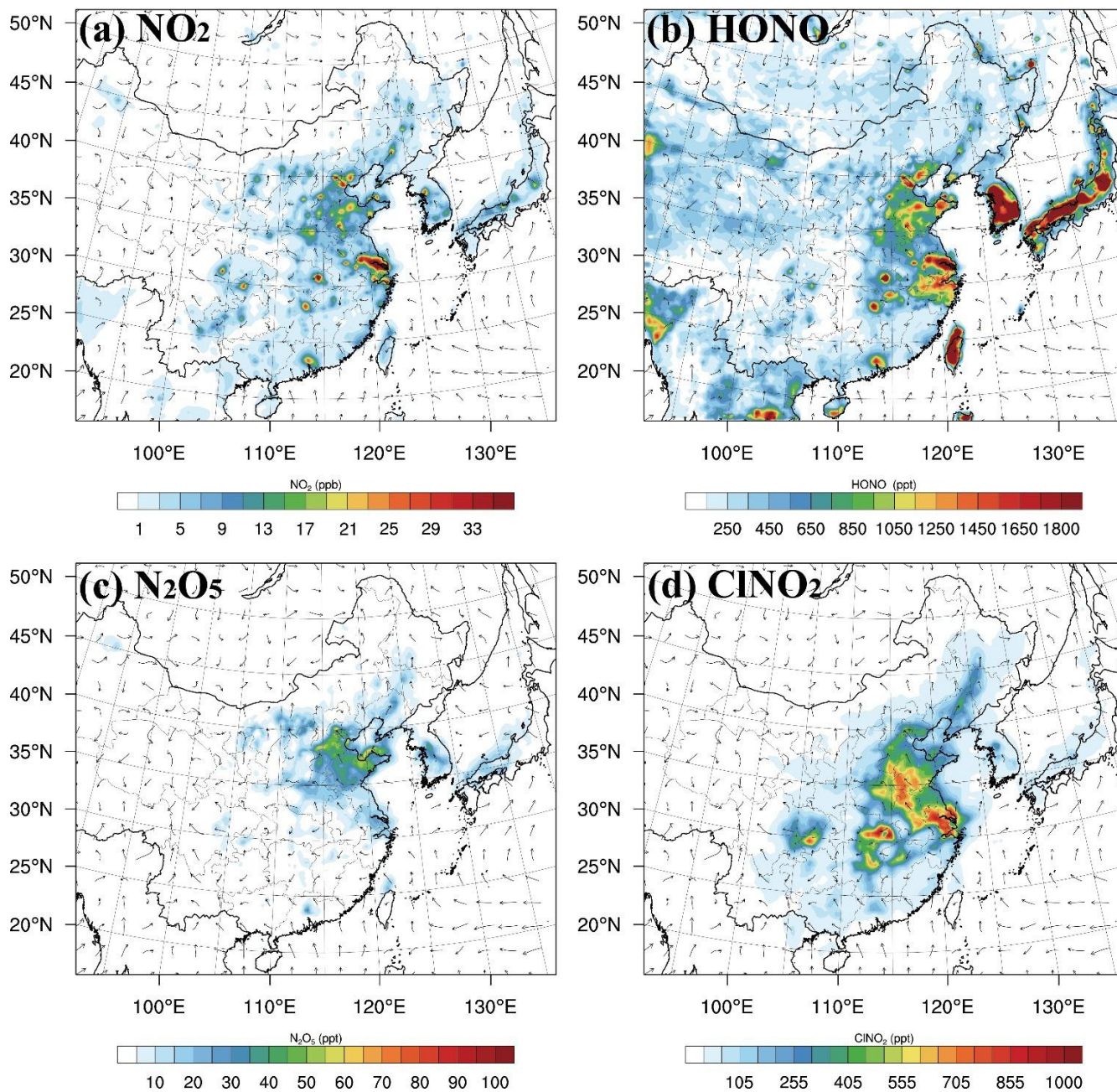
Figure 2. Spatial distributions of averaged (a) NO₂ (ppb), (b) HONO, (c) nighttime N₂O₅ (18:00–06:00 Local Time Coordinate (LTC)), and (d) nighttime ClNO₂ (ppt) in the ReNOM case at the surface (~30 m) during the simulation period (26 June-7 July 2014).
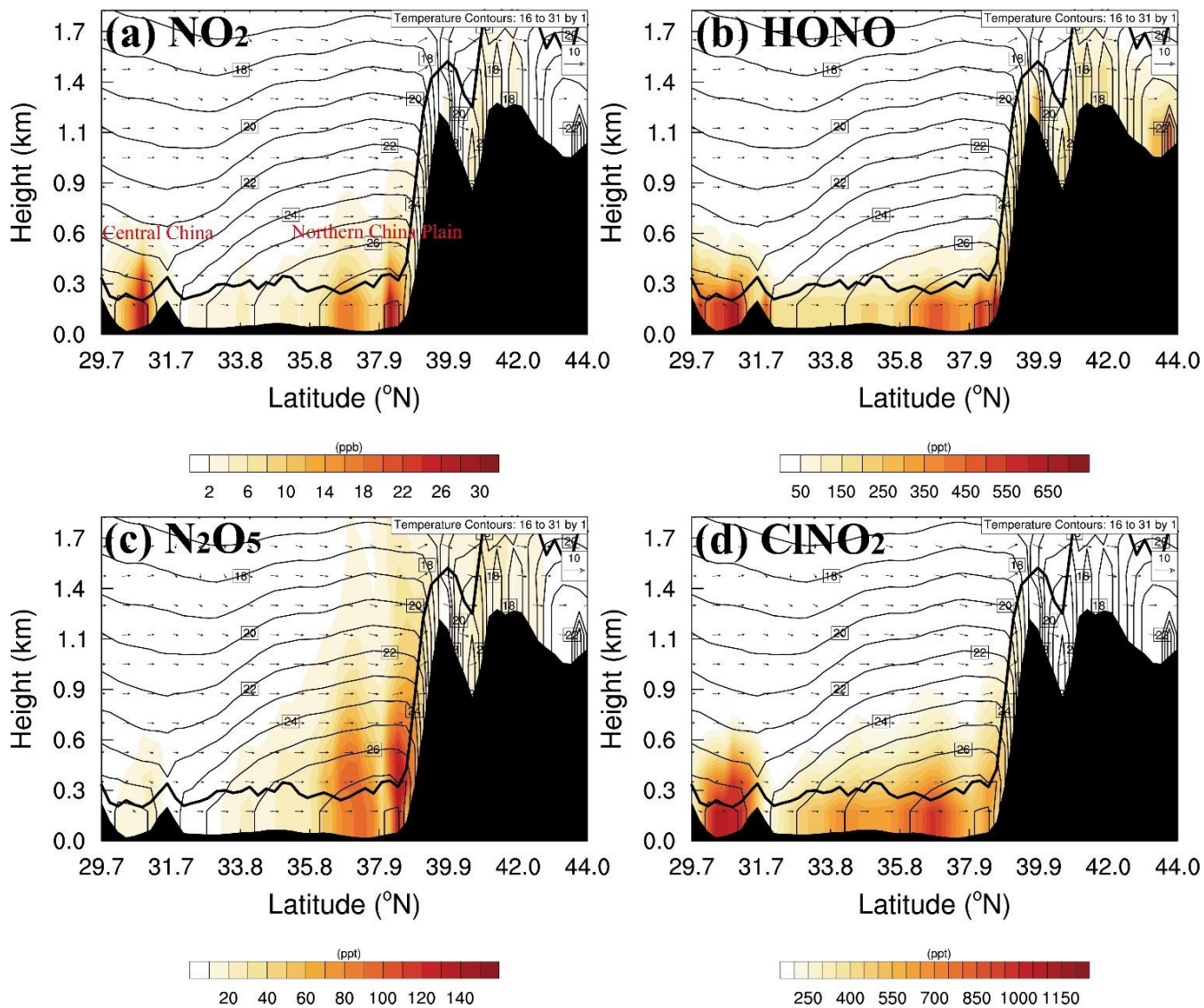
Figure 3. Vertical distributions of (a) NO$_2$ (ppb), (b) HONO, (c) N$_2$O$_5$, and (d) ClNO$_2$ (ppt) during nighttime (18:00–06:00 LTC) in the domain intercepting northern China and central China. Vectors present the average v–w wind components (m s^{-1}), the dash lines the temperature (℃), and the black line the simulated planetary boundary layer height during the nighttime.
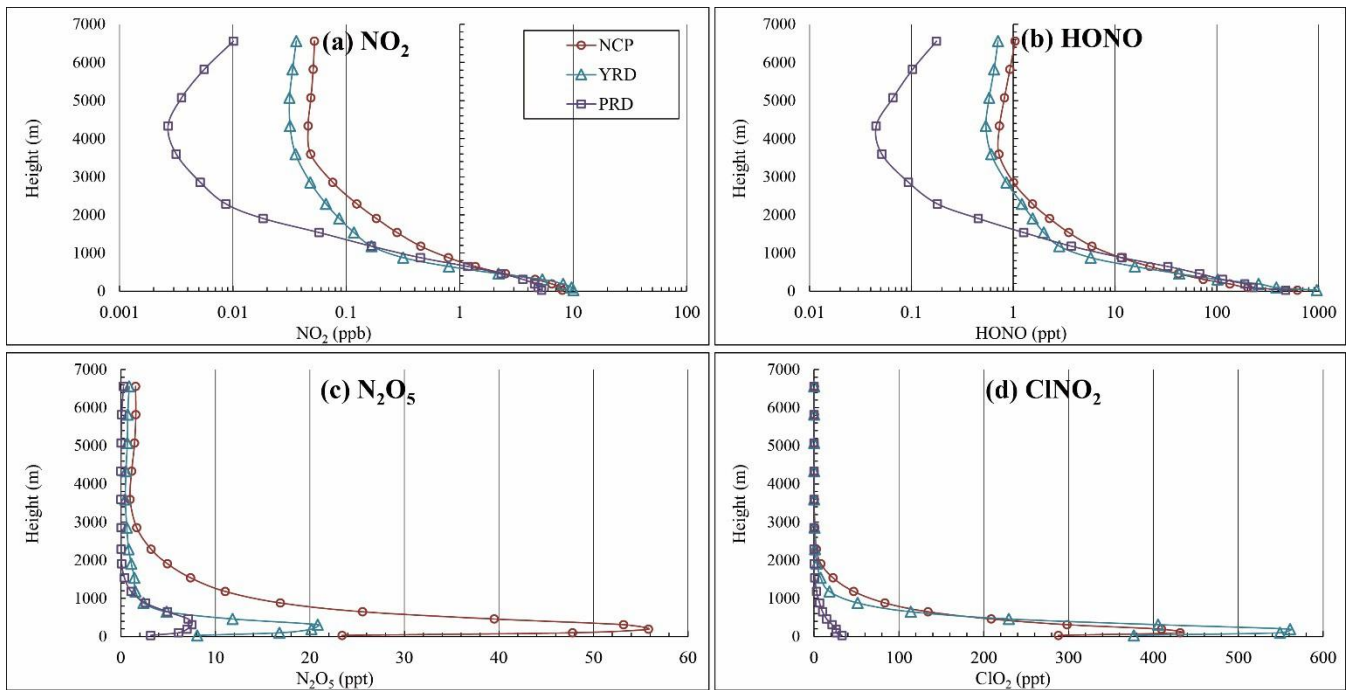
Figure 4. Vertical distributions of WRF-Chem simulated regional averages of (a) NO_2 (ppb), (b) HONO, (c) nighttime N_2O_5, and (d) nighttime $ClNO_2$ (ppt) over the NCP, YRD, and PRD regions.
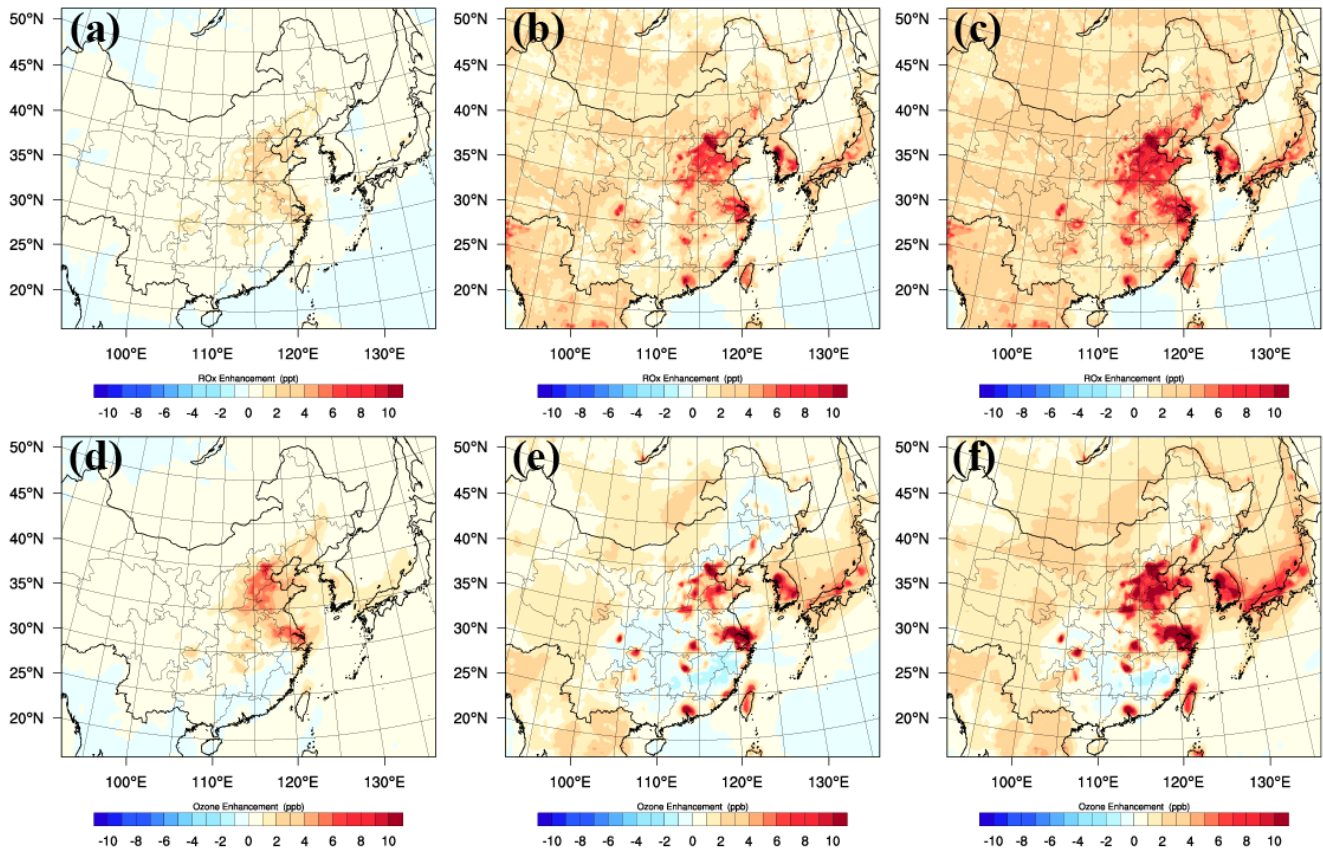
Figure 5. Daytime (06:00–18:00 LTC) RO$_x$ enhancements (ppt) in (a) ReNOM_Cl case, (b) ReNOM_HONO case, and (c) ReNOM case; O$_3$ enhancements (ppb) in (d) ReNOM_Cl case, (e) ReNOM_HONO case, and (f) ReNOM case.
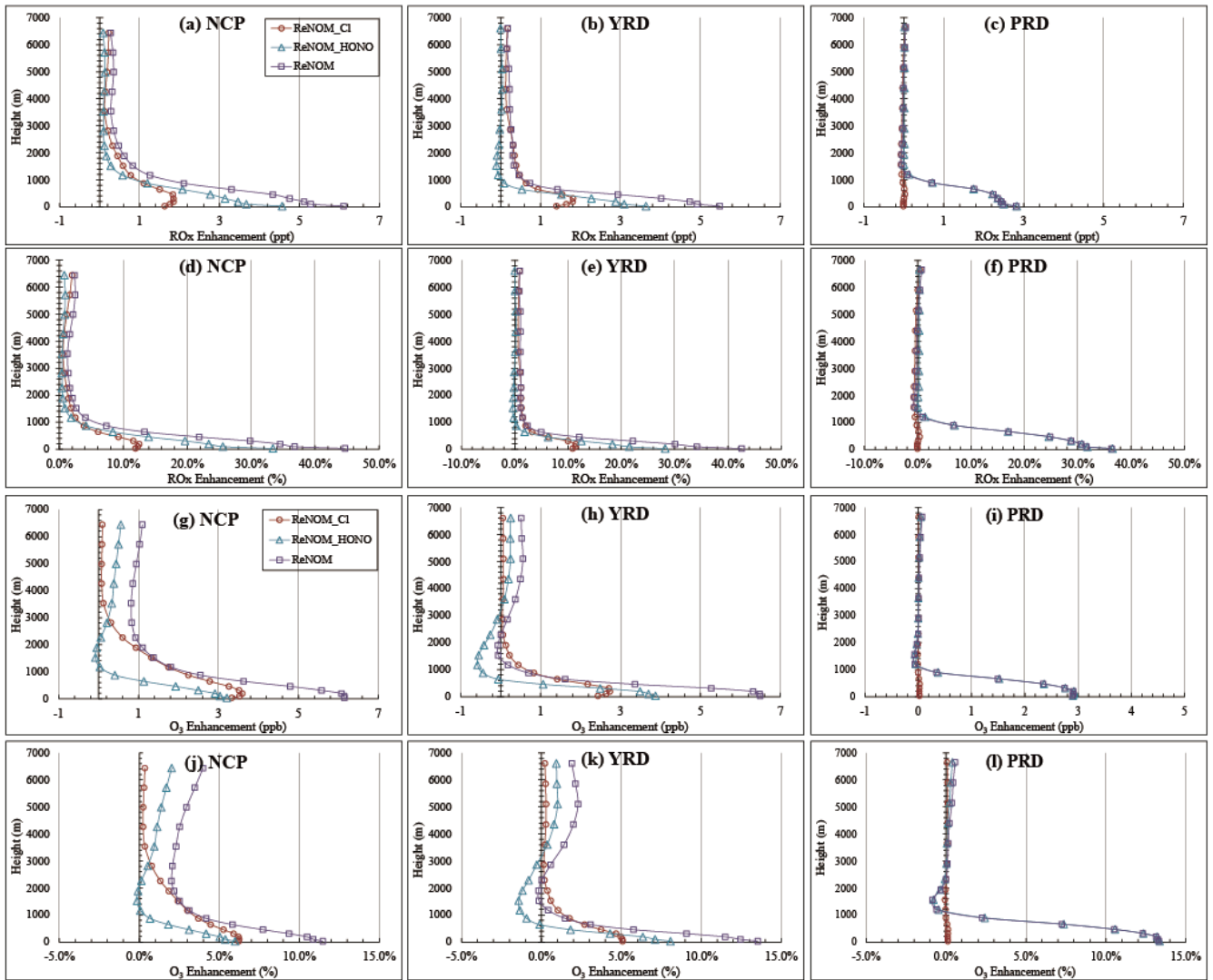
Figure 6. Daytime (06:00–18:00 LTC) vertical RO_x enhancements (ppt) over the (a) NCP, (b) YRD, and (c) PRD regions; RO_x percentage enhancements (%) over the (d) NCP, (e) YRD, and (f) PRD regions; O_3 enhancements (ppb) over the (g) NCP, (h) YRD, and (i) PRD regions; O_3 percentage enhancements (%) over the (j) NCP, (k) YRD, and (l) PRD regions.
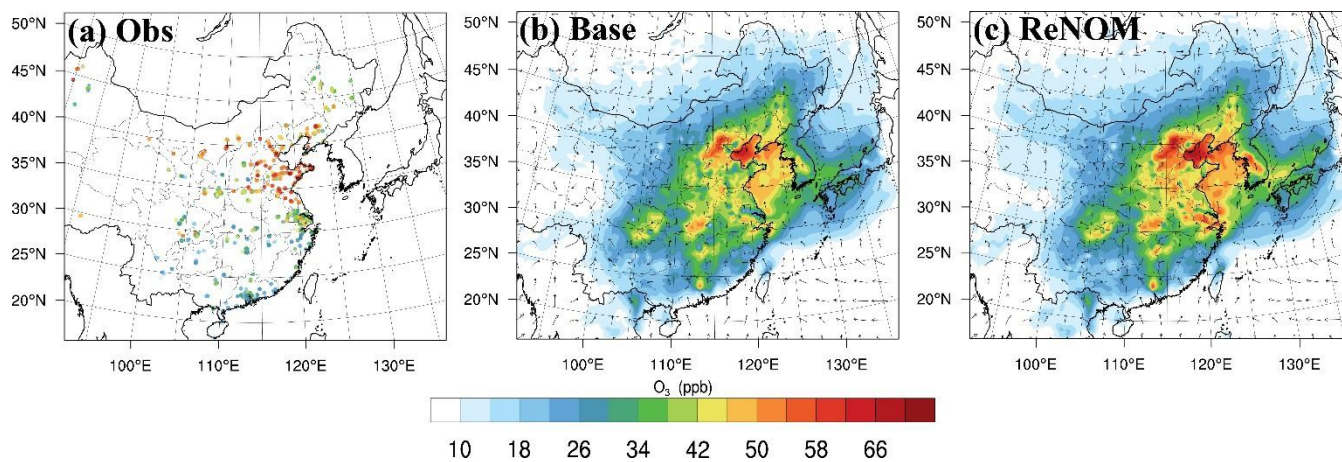
Figure 7. (a) Observations of O_3 at China MEP stations; spatial distributions of modeled O_3 concentrations in (b) base case and (c) ReNOM case (ppb).